Three Steps to Chaos—Part II: A Chua's Circuit Primer

Michael Peter Kennedy

Abstract—**Linear system theory provides an inadequate characterization of sustained oscillation in nature. In this two-part exposition of oscillation in piecewise-linear dynamical systems, we guide the reader from linear concepts and simple harmonic motion to nonlinear concepts and chaos. By means of three worked examples, we bridge the gap from the familiar parallel RLC network to exotic nonlinear dynamical phenomena in Chua's circuit. Our goal is to stimulate the reader to think deeply about the fundamental nature of oscillation and to develop intuition into the chaos-producing mechanisms of nonlinear dynamics. In order to exhibit chaos, an autonomous circuit consisting of resistors, capacitors, and inductors must contain (1) at least one nonlinear element, (2) at least one locally active resistor, and (3) at least three energy-storage elements. Chua's circuit is the simplest electronic circuit that satisfies these criteria. In addition, this remarkable circuit is the *only* physical system for which the presence of chaos has been proved mathematically. The circuit is readily constructed at low cost using standard electronic components and exhibits a rich variety of bifurcations and chaos.**

In Part I of this two-part paper, we plot the evolution of our understanding of oscillation from linear concepts and the parallel RLC resonant circuit to piecewise-linear circuits and Chua's circuit. We illustrate by theory, simulation, and laboratory experiment the concepts of equilibria, stability, local and global behavior, bifurcations, and steady-state solutions. In Part II, we study bifurcations and chaos in a robust practical implementation of Chua's circuit.

I. Introduction

Chaos is characterized by a *stretching and folding* mechanism; nearby trajectories of a dynamical system are repeatedly pulled apart exponentially and folded back together. In Part I of this tutorial paper, we saw that the steady-state solution of a second-order circuit can be either a DC equilibrium point or a limit cycle; chaos is not possible. Nevertheless, our observations of some simple two-dimensional circuits suggest how one might create the required stretching and folding mechanism. We noted how two adjacent trajectories are separated exponentially along an eigenplane by a pair of unstable complex eigenvalues. This mechanism can be exploited to provide *stretching*; *folding* may be accomplished with a third dimension and a nonlinearity.

Consider a third-order autonomous circuit described by

$$\dot{\mathbf{X}} = \mathbf{F}(\mathbf{X}), \mathbf{X}(0) = \mathbf{X}_0. \tag{1}$$

Shilnikov's theorem [1], [2], states that if an equilibrium point $\mathbf{X_Q}$ of this circuit has a pair of stable complex conjugate eigenvalues $\sigma \pm j\omega$ ($\sigma < 0$, $\omega \neq 0$) and an unstable real eigenvalue γ where $|\sigma| < |\gamma|$, and the vector field $\mathbf{F}(\mathbf{X})$ has a homoclinic orbit[1] through $\mathbf{X_Q}$, then there is a perturbation $\mathbf{F}'$ of $\mathbf{F}$ (which may be obtained by changing one or more parameters of the system) such that $\mathbf{F}'$ has *traversal homoclinic orbits* and *horseshoes*.[2] The presence of transversal homoclinic orbits implies the existence of infinitely many unstable periodic orbits of arbitrarily long period[3] as well as complicated bounded nonperiodic solutions of (1) called *chaotic* trajectories.

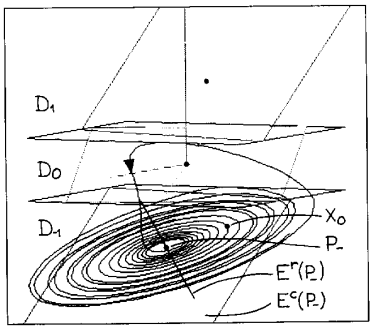

Fig. 1. Stretching and folding mechanism of chaos generation close to a homoclinic orbit in a three-region piecewise-linear vector field. A trajectory spirals away from P_- along the eigenplane $E^c(P_-)$ until it enters the D_0 region, where it is folded back into D_{-1} and returns to the unstable eigenplane $E^c(P_-)$ close to P_-.

Although we have stated it for the case $\sigma < 0, \gamma > 0$, Shilnikov's theorem also applies when the equilibrium point has an *unstable* pair of complex conjugate eigenvalues and a *stable* real eigenvalue. In that case, it is somewhat easier to visualize the stretching and folding of trajectories close to a homoclinic orbit.

Consider the trajectory of a three-region piecewise-linear vector field shown in Fig. 1. We assume that the equilibrium point P_- has a stable real eigenvalue γ_1 (whose eigenvector is $E^r(P_-)$) and an unstable complex conjugate pair of eigenvalues $\sigma_1 \pm j\omega_1$, the real and imaginary parts of

[1] A *homoclinic orbit* is the union of an equilibrium point $\mathcal{E}$ and a trajectory $\mathcal{T}$ that approaches $\mathcal{E}$ as $t \to \infty$ and as $t \to -\infty$ [1], [3]. Clearly, $\mathcal{E}$ is stable in the direction along which $\mathcal{T}$ approaches $\mathcal{E}$ as $t \to \infty$ and unstable in the direction along which $\mathcal{T}$ approaches $\mathcal{E}$ as $t \to -\infty$; an equilibrium point that is stable in one direction and unstable in another is called a *saddle*.

[2] The details of transversal homoclinic orbits and horseshoes are beyond the scope of this paper; we refer the reader to [1] for a rigorous treatment of these topics.

[3] Well-behaved periodic motion with any desired period can be obtained from a chaotic system by stabilizing an unstable periodic orbit of the desired length [4].

Manuscript received April 1, 1993; revised manuscript received June 22, 1993. This paper was recommended by Guest Editor L. O. Chua.

The author is with the Department of Electronic and Electrical Engineering, University College Dublin, Republic of Ireland.

IEEE Log Number 9211603.

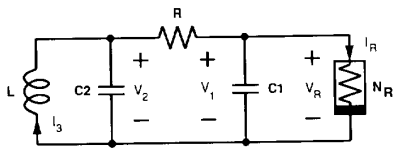

Fig. 2. Chua's circuit consists of a linear inductor L, two linear capacitors (C_2, C_1), a linear resistor R, and a voltage-controlled nonlinear resistor N_R.

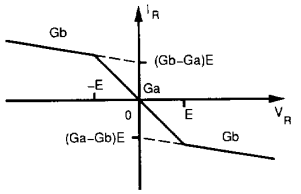

Fig. 3. The driving-point characteristic of the nonlinear resistor N_R in Chua's circuit has breakpoints at $\pm E$ and slopes G_a and G_b in the inner and outer regions, respectively.

whose eigenvectors span the plane $E^c(P_-)$ [5], as shown. A trajectory originating from a point $\mathbf{X}_0$ on $E^c(P_-)$ spirals away from the equilibrium point along $E^c(P_-)$ until it enters the D_0 region, where it is folded back into D_{-1}. Upon reentering D_{-1}, the trajectory is pulled toward P_- roughly in the direction of the real eigenvector $E^r(P_-)$, as shown.

Now imagine what would happen if the trajectory entering D_{-1} from D_0 were in *precisely* the direction $E^r(P_-)$. Such a trajectory would follow $E^r(P_-)$ toward P_-, reaching the equilibrium point asymptotically as $t \to \infty$. Similarly, if we were to follow this trajectory *backward* in time though D_0 and back onto $E^c(P_-)$ in D_{-1}, it would then spiral toward P_-, reaching it asymptotically as $t \to -\infty$. The trajectory thus formed would be a homoclinic orbit, reaching the same equilibrium point P_- asymptotically in forward and reverse time.

While the homoclinic orbit itself is not structurally stable, and therefore cannot be observed experimentally, it is indicative of complicated dynamical behavior nearby [1]. In this example, we see that a trajectory lying close to the postulated homoclinic orbit exhibits similar qualitative behavior: it spirals away from P_- along the unstable complex plane $E^c(P_-)$, is folded in D_0, reenters D_{-1} above $E^c(P_-)$, and is pulled back toward $E^c(P_-)$ only to be spun away from P_- once more. Thus, two trajectories starting from distinct initial states close to P_- on $E^c(P_-)$ are stretched apart exponentially along the unstable eigenplane before being folded in D_1 and reinjected close to P_-. This recurrent stretching and folding continues *ad infinitum*, producing a chaotic steady-state solution.

The Genesis of Chua's Circuit

While on a visit to Japan in 1983, having witnessed a futile attempt at producing chaos in an electrical analog of Lorenz's equations, Leon Chua was prompted to develop a chaotic electronic circuit. He realized that chaos could be produced in a piecewise-linear circuit if it possessed at least two unstable equilibrium points—one to provide stretching, and the other to fold trajectories. With this insight, he systematically identified those third-order piecewise-linear circuits containing a single voltage-controlled nonlinear resistor that could produce chaos. Specifying that the driving-point (DP) characteristic of the voltage-controlled nonlinear resistor N_R should be chosen to yield at least *two* unstable equilibrium points, he invented the circuit shown in Fig. 2.

Let the nonlinear resistor N_R in Chua's circuit have a piecewise-linear DP characteristic as shown in Fig. 3. Imagine that the values of the parameters are chosen such that the circuit possesses three equilibrium points (one at the origin with locally negative slope or *conductance* G_a, and two in the outer regions with locally negative conductance G_b) and that all three equilibrium points are *unstable*. Associated with each equilibrium point are three eigenvalues. We assume that the equilibrium point at the origin has an *unstable* real eigenvalue and a *stable* pair of complex conjugate eigenvalues; we saw in Section VI of Part I that this is possible. In addition, suppose that the outer equilibrium point P_- has a *stable* real eigenvalue and an *unstable* complex pair. Two trajectories starting close together on the eigenplane in the outer region would be stretched apart as they spiralled away from the equilibrium point. If they could be *folded* back by the dynamics in the inner region and reinjected toward P_- along the stable real eigenvector, a *homoclinic orbit* would be produced, and chaos would result.

Soon after its conception, the rich dynamical behavior of Chua's circuit was confirmed by computer simulation [6] and experiment [7]. Since then, there has been an intensive effort to understand every aspect of the dynamics of this circuit with a view to developing it as a paradigm for learning, understanding, and teaching about nonlinear dynamics and chaos.

That the circuit does in fact exhibit chaos in the sense of Shilnikov was proved by Chua *et al.* in 1986 [2]. More recently, by adding a linear resistor in series with the inductor, the circuit has been generalized to the canonical *Chua's oscillator* [8]. This circuit is canonical in the sense that every continuous three-dimensional odd-symmetric piecewise-linear vector field may be mapped onto the circuit. The circuit can thus exhibit *every dynamical behavior* known to be possible in a system described by a continuous odd-symmetric three-region piecewise-linear vector field. With the appropriate choice of parameters, the circuit can be made to follow the classic *period-doubling, intermittency*, and *torus breakdown* routes to chaos. For a comprehensive bibliography of papers on Chua's circuit, we refer the reader to Chua's historical review paper [9].

II. Chua's Circuit

In Part I of this two-part paper, we plotted (with hindsight) the evolution of Chua's circuit from the classic parallel RLC resonant circuit. From periodic motion and two-dimensional dynamics, we learned about piecewise-linear analysis and three-dimensional dynamics. In Part II, we study in detail the geometry and state-space dynamics of Chua's circuit. We concentrate on a particular set of parameters and behaviors which are readily reproducible by simulation and experiment.

In order to produce at least *two* unstable equilibrium points without sacrificing the benefits of piecewise-linear analysis, we specify a piecewise-linear DP characteristic for the nonlinear resistor N_R, as shown in Fig. 3. This characteristic is defined analytically as follows:

$$I_R = f(V_R) = \begin{cases} G_b V_R + (G_b - G_a)E & \text{if} \quad V_R < -E \\ G_a V_R & \text{if} \quad -E \leq V_R \leq E \\ G_b V_R + (G_a - G_b)E & \text{if} \quad V_R > E \end{cases}$$

where $E > 0$, $G_a < 0$, and $G_b < 0$. In contrast with the nonlinear resistor considered in Part I, note that G_a and G_b are now *both* negative.

Piecewise-Linear Description of Chua's Circuit

We have seen that this circuit may be described by three ordinary differential equations (state equations). Choosing I_3, V_2 and V_1 as *state variables*, we write the equations shown in (2), (3), and (4) at the bottom of this page, where $G = 1/R$, $G'_a = G + G_a$ and $G'_b = G + G_b$.

Because of the piecewise-linear nature of N_R, the vector field of Chua's circuit may be decomposed into three distinct affine regions: $V_1 < -E$, $|V_1| \leq E$, and $V_1 > E$. We call these the D_{-1}, D_0, and D_1 regions, respectively. Using piecewise-linear analysis, we examine each region separately, and then glue the pieces together. First, we review some results concerning linear algebra and ordinary differential equations.

Eigenvalues and Eigenvectors Revisited

Consider the three-dimensional autonomous affine dynamical system

$$\dot{\mathbf{X}}(t) = \mathbf{A}\mathbf{X}(t) + \mathbf{b}, \mathbf{X}(0) = \mathbf{X}_0, \tag{5}$$

where $\mathbf{A}$ is the (constant) system matrix and $\mathbf{b}$ is a constant vector. $\mathbf{X}(t)$ is a trajectory originating from the initial state $\mathbf{X}_0$. We saw in Part I that the equilibrium point $\mathbf{X_Q}$ of this system is defined by

$$\mathbf{X_Q} = -\mathbf{A}^{-1}\mathbf{b},$$

if $\mathbf{A}^{-1}$ exists, and that the dynamics close to $\mathbf{X_Q}$ are governed locally by the linear system

$$\dot{\mathbf{x}}(t) = \mathbf{J}\mathbf{x}(t) \tag{6}$$

where $\mathbf{J}$ is simply the system matrix $\mathbf{A}$ in the case of a linear or affine system.

If the eigenvalues λ_1, λ_2, and λ_3 of $\mathbf{J}$ are *distinct*, then every solution $\mathbf{x}(t)$ of (6) may be expressed in the form

$$\mathbf{x}(t) = c_1 \exp(\lambda_1 t)\vec{\xi}_1 + c_2 \exp(\lambda_2 t)\vec{\xi}_2 + c_3 \exp(\lambda_3 t)\vec{\xi}_3,$$

where $\vec{\xi}_1$, $\vec{\xi}_2$, and $\vec{\xi}_3$ are the (possibly complex) eigenvectors associated with the eigenvalues λ_1, λ_2, and λ_3, respectively, and the c_k's are (possibly complex) constants that depend on the initial state $\mathbf{X}_0$ [10].

In the special case when $\mathbf{J}$ has one real eigenvalue γ and a complex conjugate pair of eigenvalues$\sigma \pm j\omega$, the solution of (6) has the form:

$$\mathbf{x}(t) = C_r \exp(\gamma t)\vec{\xi}_\gamma + 2c_c \exp(\sigma t)[\cos(\omega t + \phi_c)\vec{\eta}_r - \sin(\omega t + \phi_c)\vec{\eta}_i]$$

where $\vec{\eta}_r$ and $\vec{\eta}_i$ are the real and imaginary parts of the eigenvectors associated with the complex conjugate pair of eigenvalues, $\vec{\xi}_\gamma$ is the eigenvector defined by $\mathbf{J}\vec{\xi}_\gamma = \gamma\vec{\xi}_\gamma$, and c_r, c_c, and ϕ_c are real constants that are determined by the initial conditions.

Let us relabel the real eigenvector E^r and define E^c as the complex eigenplane spanned by $\vec{\eta}_r$ and $\vec{\eta}_i$.

We can think of the solution $\mathbf{x}(t)$ of (6) as being the sum of two distinct components $\mathbf{x}_r(t) \in E^r$ and $\mathbf{x}_c(t) \in E^c$:

$$\mathbf{x}_r(t) = c_r \exp(\gamma t)\vec{\xi}_\gamma$$
$$\mathbf{x}_c(t) = 2c_c \exp(\sigma t)[\cos(\omega t + \phi_c)\vec{\eta}_r - \sin(\omega t + \phi_c)\vec{\eta}_i].$$

Because the Jacobian matrix of an affine system is simply the system matrix $\mathbf{A}$, the complete solution $\mathbf{X}(t)$ of (5) may be found by translating the origin of the linearized coordinate system to the equilibrium point $\mathbf{X_Q}$. Thus,

$$\begin{aligned} \mathbf{X}(t) &= \mathbf{X_Q} + \mathbf{x}(t) \\ &= \mathbf{X_Q} + \mathbf{x}_r(t) + \mathbf{x}_c(t). \end{aligned}$$

We can determine the qualitative behavior of the complete solution $\mathbf{X}(t)$ by considering separately the components $\mathbf{x}_r(t)$ and $\mathbf{x}_c(t)$ along E^r and E^c, respectively.

If $\gamma > 0$, $\mathbf{x}_r(t)$ grows exponentially in the direction of E^r; if $\gamma < 0$, $\mathbf{x}_r(t)$ tends asymptotically to zero. When $\sigma > 0$ and $\omega \neq 0$, $\mathbf{x}_c(t)$ spirals away from $\mathbf{X_Q}$ along the complex eigenplane E^c, and if $\sigma < 0$, $\mathbf{x}_c(t)$ spirals toward $\mathbf{X_Q}$ along E^c.

$$\frac{dI_3}{dt} = -\frac{1}{L}V_2 \tag{2}$$

$$\frac{dV_2}{dt} = \frac{1}{C_2}I_3 - \frac{G}{C_2}(V_2 - V_1) \tag{3}$$

$$\frac{dV_1}{dt} = \frac{G}{C_1}(V_2 - V_1) - \frac{1}{C_1}f(V_1) = \begin{cases} \frac{G}{C_1}V_2 - \frac{G'_b}{C_1}V_1 - \left(\frac{G_b - G_a}{C_1}\right)E & \text{if} \quad V_1 < -E \\ \frac{G}{C_1}V_2 - \frac{G'_a}{C_1}V_1 & \text{if} \quad -E \leq V_1 \leq E \\ \frac{G}{C_1}V_2 - \frac{G'_b}{C_1}V_1 - \left(\frac{G_a - G_b}{C_1}\right)E & \text{if} \quad V_1 > E \end{cases} \tag{4}$$

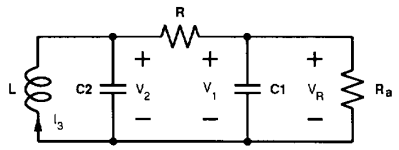

Fig. 4. Equivalent circuit of Chua's circuit (Fig. 2) in the D_0 region. $R_a = 1/G_a$.

We remark that the vector E^r and plane E^c are *invariant* under the flow (5). If $\mathbf{X}(0) \in E^r$, then $\mathbf{X}(t) \in E^r$ for all t; if $\mathbf{X}(0) \in E^c$, then $\mathbf{X}(t) \in E^c$ for all t. An important consequence of this is that a trajectory $\mathbf{X}(t)$ cannot *cross* through the complex eigenspace E^c. Suppose $\mathbf{X}(t_0) \in E^c$ at some time t_0; then $\mathbf{X}(t) \in E^c$ for all $t > t_0$.

A state $\mathbf{X} \in \mathbb{R}^3$ lies on the plane E^c if $(\mathbf{X} - \mathbf{X_Q}) \cdot \mathbf{n} = 0$, where $\cdot$ denotes the dot product and $\mathbf{n}$ is the *normal* vector, which is perpendicular to E^c. Thus, the plane E^c through an equilibrium point $\mathbf{X_Q}$ is characterized by the normal vector $\mathbf{n}$.

We are now ready to examine the dynamics of Chua's circuit in each region. We look at D_0 first.

The Middle Region ($|V_1| \leq E$)

When $|V_1| \leq E$, Chua's circuit is described by

$$\begin{aligned}\frac{dI_3}{dt} &= -\frac{1}{L}V_2 \\ \frac{dV_2}{dt} &= \frac{1}{C_2}I_3 - \frac{G}{C_2}(V_2 - V_1) \\ \frac{dV_1}{dt} &= \frac{G}{C_1}V_2 - \frac{G'_a}{C_1}V_1\end{aligned}$$

The D_0 equivalent circuit is simply the linear parallel RLC circuit shown in Fig. 4.

This linear circuit has a single equilibrium point at the origin whose stability is completely specified by the eigenvalues of

$$\mathbf{J_{F_a}} = \begin{bmatrix} 0 & -\frac{1}{L} & 0 \\ \frac{1}{C_2} & -\frac{G}{C_2} & \frac{G}{C_2} \\ 0 & \frac{G}{C_1} & -\frac{G'_a}{C_1} \end{bmatrix}$$

namely, the zeros of the characteristic polynomial

$$\lambda^3 + \left(\frac{G}{C_2} + \frac{G'_a}{C_1}\right)\lambda^2 + \left(\frac{1}{LC_2} + \frac{GG_a}{C_1C_2}\right)\lambda + \frac{G'_a}{LC_1C_2}$$

Throughout this paper, we consider a fixed set of component values: $L = 18$ mH, $C_2 = 100$ nF, $C_1 = 10$ nF, $G_a = -55/60$ mS $= -757.576\mu$S, $G_b = -9/22$ mS $= -409.091\mu$S, and $E = 1$ V.

When $G = 550\mu$S, the eigenvalues of $\mathbf{J_{F_a}}$ are:

$$\begin{aligned}\gamma_0 &\approx 25291 \\ \sigma_0 \pm j\omega_0 &\approx -5842 \pm j19720\end{aligned}$$

Associated with the unstable real eigenvalue γ_0 in the D_0 region is an eigenvector $E^r(0)$ that is defined by

$$\mathbf{J_{F_a}}E^r(0) = \gamma_0 E^r(0).$$

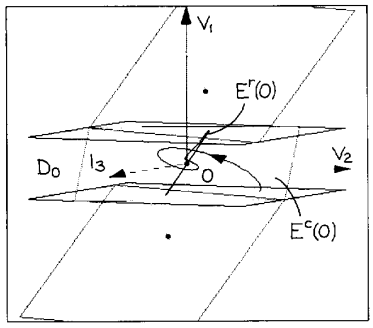

Fig. 5. Dynamics of the D_0 region. A trajectory starting slightly above the stable complex eigenplane $E^c(0)$ spirals toward the origin along this plane and is repelled close to 0 in the direction of the unstable eigenvector $E^r(0)$.

Writing $E^r(0) = [x, y, z]^T$, we have

$$\begin{bmatrix} \gamma_0 & \frac{1}{L} & 0 \\ -\frac{1}{C_2} & \gamma_0 + \frac{G}{C_2} & -\frac{G}{C_2} \\ 0 & -\frac{G}{C_1} & \gamma_0 + \frac{G'_a}{C_1} \end{bmatrix} \begin{bmatrix} x \\ y \\ z \end{bmatrix} = \begin{bmatrix} 0 \\ 0 \\ 0 \end{bmatrix}$$

Normalized to $z = 1$, the corresponding eigenvector is:

$$E^r(0) = \begin{bmatrix} x \\ y \\ z \end{bmatrix} = \begin{bmatrix} \left(\gamma_0 + \frac{G}{C_2}\right)\left(\gamma_0 + \frac{G'_a}{C_1}\right)\frac{C_1C_2}{G} - G \\ \frac{C_1}{G}\left(\gamma_0 + \frac{G'_a}{C_1}\right) \\ 1 \end{bmatrix}$$

The real and imaginary parts of the complex eigenvectors associated with $\sigma_0 \pm j\omega_0$ span a *complex eigenplane*, which we denote by $E^c(0)$. The vector normal to $E^c(0)$ is

$$\begin{bmatrix} -\frac{LC_2}{G}\left(\gamma_0 + \frac{G'_a}{C_1}\right)\left(\gamma_0 + \frac{G}{C_2}\right) + \frac{LG}{C_1} \\ \frac{C_2}{G}\left(\gamma_0 + \frac{G'_a}{C_1}\right) \\ 1 \end{bmatrix} = \begin{bmatrix} -\frac{L}{C_1}x \\ \frac{C_2}{C_1}y \\ z \end{bmatrix}$$

where γ_0 is the *real* eigenvalue in D_0.

This plane is characterized by the fact that for every $\mathbf{X} \in E^c(0)$, $\mathbf{J_{F_a}X} \in E^c(0)$. Thus, a trajectory starting on the eigenplane $E^c(0)$ evolves along $E^c(0)$. We remarked earlier that a trajectory cannot cross through an eigenplane. An important consequence of this is that a trajectory that originates from an initial state above the eigenplane remains indefinitely above the plane, and one that originates below $E^c(0)$ remains forever below the plane.

Qualitative Description of the D_0 Dynamics: A trajectory starting from some initial state $\mathbf{X}_0$ in the D_0 region may be decomposed into its components along the complex eigenplane $E^c(0)$ and along the eigenvector $E^r(0)$. When $\gamma_0 > 0$ and $\sigma_0 < 0$, the component along $E^c(0)$ spirals toward the origin along this plane while the component in the direction $E^r(0)$ grows exponentially. Adding the two components, we see that a trajectory starting slightly above the stable complex eigenplane $E^c(0)$ spirals toward the origin along the $E^c(0)$ direction, all the while being pushed away from $E^c(0)$ along the unstable direction $E^r(0)$. As the (stable) component along $E^c(0)$ shrinks in magnitude, the unstable component grows exponentially, and the trajectory follows a helix of exponentially decreasing radius whose axis lies in the direction of $E^r(0)$; this is illustrated in Fig. 5.

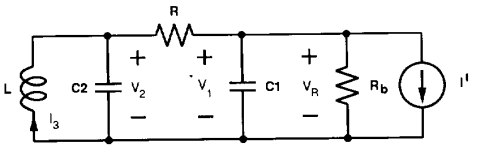

Fig. 6. Equivalent circuit of Fig. 2 in the D_1 region. $R_b = 1/G_b$. $I' = (G_b - G_a)E$ when $V_1 < -E$ and $I' = (G_a - G_b)E$ when $V_1 > E$.

The Outer Regions ($|V_1| > E$)

In the outer regions, Chua's circuit (with a piecewise-linear N_R) is described by

$$\begin{aligned}\frac{dI_3}{dt} &= -\frac{1}{L}V_2 \\ \frac{dV_2}{dt} &= \frac{1}{C_2}I_3 - \frac{G}{C_2}(V_2 - V_1) \\ \frac{dV_1}{dt} &= \frac{G}{C_1}V_2 - \frac{G_b'}{C_1}V_1 - \frac{I'}{C_1}\end{aligned} \tag{7}$$

where $I' = (G_b - G_a)E$ when $V_1 < -E$ (the D_{-1} region) and $I' = (G_a - G_b)E$ when $V_1 > E$ (the D_1 region). The D_{-1} and D_1 affine equivalent circuits[4] consist of a linear parallel RLC circuit with resistance $R_b' = 1/G_b'$ and a shunt DC current source I', as shown in Fig. 6.

The equilibrium points P_- and P_+ of the outer regions are given by $V_2 = 0$, $V_1 = -I'/G_b'$, and $I_3 = -GV_1 = I'G/G_b'$. Note that an equilibrium point is simply a DC solution of the equivalent circuit and may be determined by short-circuiting L and open-circuiting C_1 and C_2 [5]. The equilibrium points of the outer regions are thus

$$P_- = \begin{bmatrix} \frac{G(G_b - G_a)E}{G+G_b} \\ 0 \\ \frac{(G_a - G_b)E}{G+G_b} \end{bmatrix}, P_+ = \begin{bmatrix} \frac{G(G_a - G_b)E}{G+G_b} \\ 0 \\ \frac{(G_b - G_a)E}{G+G_b} \end{bmatrix}$$

If the equilibrium point P_- lies *outside* the D_{-1} region, then it is called a *virtual* equilibrium point [5]. While this is a valid solution of the affine D_{-1} equivalent circuit described by (7), it is not an equilibrium point of the circuit itself. For example, the equilibrium point P_- lies *outside* D_{-1} (and so is a virtual equilibrium point) if

$$\frac{(G_a - G_b)E}{G + G_b} > -E$$

. Equivalently, the point P_- is an equilibrium point of Fig. 2 (when $G > 0$) only if $-G_b < G < -G_a$.

We can determine the stability of the equilibrium points and the dynamics of the outer regions by examining the Jacobian matrix

$$\mathbf{J_{Fb}} = \begin{bmatrix} 0 & -\frac{1}{L} & 0 \\ \frac{1}{C_2} & -\frac{G}{C_2} & \frac{G}{C_2} \\ 0 & \frac{G}{C_1} & -\frac{G_b'}{C_1} \end{bmatrix}$$

whose eigenvalues are the zeroes of the characteristic polynomial

$$\lambda^3 + \left(\frac{G}{C_2} + \frac{G_b'}{C_1}\right)\lambda^2 + \left(\frac{1}{LC_2} + \frac{GG_b}{C_1C_2}\right)\lambda + \frac{G_b'}{LC_1C_2}$$

[4]The D_{-1} and D_1 equivalent circuits are not small-signal (local) equivalent circuits; they model the *large-signal* (global) behavior of the system in the outer regions.

With all other component values as before, and $G = 550\mu$S, the eigenvalues of $\mathbf{J_{Fb}}$ are:

$$\gamma_1 \approx -23284$$
$$\sigma_1 \pm j\omega_1 \approx 1022 \pm j19260$$

Associated with the stable real eigenvalue γ_1 in the D_1 region is an eigenvector $E^r(P_+)$, which is defined by

$$\mathbf{J_{Fb}}E^r(P_+) = \gamma_1 E^r(P_+).$$

Writing $E^r(P_+) = [x, y, z]^T$, we have

$$\begin{bmatrix} \gamma_1 & \frac{1}{L} & 0 \\ -\frac{1}{C_2} & \gamma_1 + \frac{G}{C_2} & -\frac{G}{C_2} \\ 0 & -\frac{G}{C_1} & \gamma_1 + \frac{G_b'}{C_1} \end{bmatrix} \begin{bmatrix} x \\ y \\ z \end{bmatrix} = \begin{bmatrix} 0 \\ 0 \\ 0 \end{bmatrix}$$

Normalized to $z = 1$, the real eigenvector is:

$$E^r(P_+) = \begin{bmatrix} x \\ y \\ z \end{bmatrix} = \begin{bmatrix} \left(\gamma_1 + \frac{G}{C_2}\right)\left(\gamma_1 + \frac{G_b'}{C_1}\right)\frac{C_1C_2}{G} - G \\ \frac{C_1}{G}\left(\gamma_1 + \frac{G_b'}{C_1}\right) \\ 1 \end{bmatrix}$$

The real and imaginary parts of the complex eigenvectors associated with $\sigma_1 \pm j\omega_1$ span a complex eigenplane, which we denote $E^c(P_+)$. The vector normal to $E^c(P_+)$ is

$$\begin{bmatrix} -\frac{LC_2}{G}\left(\gamma_1 + \frac{G_b'}{C_1}\right)\left(\gamma_1 + \frac{G}{C_2}\right) + \frac{LG}{C_1} \\ \frac{C_2}{G}\left(\gamma_1 + \frac{G_b'}{C_1}\right) \\ 1 \end{bmatrix} = \begin{bmatrix} -\frac{L}{C_1}x \\ \frac{C_2}{C_1}y \\ z \end{bmatrix}$$

where γ_1 is the *real* eigenvector in D_1.

This eigenplane is characterized by the fact that for every $\mathbf{X} \in E^c(P_+)$, $\mathbf{J_{Fb}X} \in E^c(P_+)$ so a trajectory starting on $E^c(P_+)$ evolves along $E^c(P_+)$. Once again, we note that a trajectory that originates from an initial state above the complex eigenplane remains indefinitely above the plane, and one that originates below remains below.

Qualitative Description of the Dynamics for $|V_1| > E$: Associated with the stable real eigenvalue γ_1 in the D_1 region is the eigenvector $E^r(P_+)$. The real and imaginary parts of the complex eigenvectors associated with $\sigma_1 \pm j\omega_1$ define a complex eigenplane $E^c(P_+)$.

A trajectory starting from some initial state $\mathbf{X}_0$ in the D_1 region may be decomposed into its components along the complex eigenplane $E^c(P_+)$ and the eigenvector $E^r(P_+)$. When $\gamma_1 < 0$ and $\sigma_1 > 0$, the component on $E^c(P_+)$ spirals away from P_+ along this plane while the component in the direction of $E^r(0)$ tends asymptotically toward P_+. Adding the two components, we see that a trajectory starting close to the stable real eigenvector $E^r(P_+)$ above the complex eigenplane moves toward $E^c(P_+)$ along a helix of exponentially increasing radius. Since the component along $E^r(P_+)$ shrinks exponentially in magnitude and the component on $E^c(P_+)$ grows exponentially, the trajectory is quickly flattened onto $E^c(P_+)$, where it spirals away from P_+ along the complex eigenplane; this is illustrated in Fig. 7.

Note that because of the strong rate of contraction along the $E^r(P_+)$ direction, a trajectory spends most of its time in D_1 coasting very close to $E^c(P_+)$. Consequently, the system appears locally to be two-dimensional and can therefore be

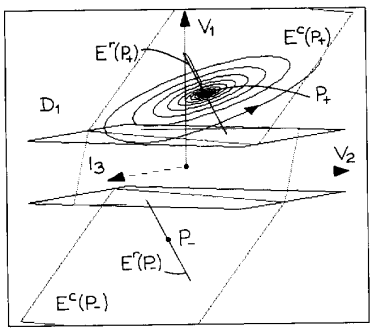

Fig. 7. Dynamics of the D_1 region. A trajectory starting above the unstable complex eigenplane $E^c(P_+)$ close to the eigenvector $E^r(P_+)$ moves toward the plane and spirals away from P_+ along $E^c(P_+)$. By symmetry, the D_{-1} region has equivalent dynamics.

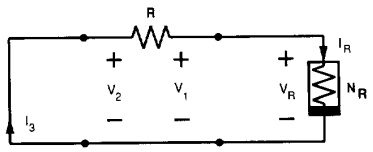

Fig. 8. dc equivalent circuit of Fig. 2 obtained by short-circuiting the inductor L and open-circuiting capacitors C_1 and C_2.

readily analyzed by using one-dimensional discrete maps (see, e.g., [11]).

By symmetry, the equilibrium point P_- in the D_{-1} region has three eigenvalues: γ_1 and $\sigma_1 \pm j\omega_1$. The eigenvector $E^r(P_-)$ is associated with the stable real eigenvalue γ_1; the real and imaginary parts of the eigenvectors associated with the unstable complex pair $\sigma_1 \pm j\omega_1$ define an eigenplane $E^c(P_-)$ along which trajectories spiral away from P_-.

Global Behavior

The global dynamics of Chua's circuit may be determined by piecing together the three-dimensional vector fields of the three regions D_{-1}, D_0, and D_1.

The equilibrium points of the entire circuit are defined by

$$0 = -\frac{1}{L}V_2$$
$$0 = \frac{1}{C_2}I_3 - \frac{G}{C_2}(V_2 - V_1)$$
$$0 = \frac{G}{C_1}(V_2 - V_1) - \frac{1}{C_1}I_R$$

Equivalently, one open-circuits the capacitors C_1 and C_2, and short-circuits the inductor L to find the dc solutions. This is illustrated in Fig. 8. Clearly, the dc solution of this circuit is $I_R = -GV_R$. The equilibrium points may be determined graphically by intersecting the *load line* $I_R = -GV_R$ with the DP characteristic $I_R = f(V_R)$ of the nonlinear resistor N_R, as shown in Fig. 9 [5]. When $G > |G_a|$ or $G < |G_b|$, the circuit has a unique equilibrium point at the origin (and two virtual equilibria P_- and P_+); otherwise, it has three equilibrium points at $P_-, 0$, and P_+.

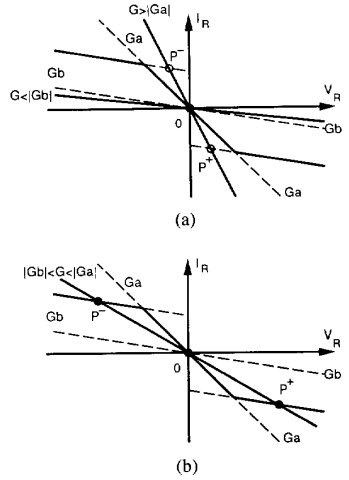

Fig. 9. dc equilibrium points of Fig. 2 may be determined graphically by intersecting the load line $I_R = -GV_R$ with the DP characteristic of N_R. (a) If $G > |G_a|$ or $G < |G_b|$, the circuit has a unique equilibrium point at the origin (P_- and P_+ are *virtual equilibria* in this case). (b) When $|G_b| < G < |G_a|$, the circuit has three equilibrium points at $P_-, 0$, and P_+.

In the following discussion, we consider the global behavior of the circuit using our chosen set of parameters with R in the range $0 \leq R \leq 2000\Omega$ ($500\mu\text{S} \leq G < \infty$ S).

Fig. 10 is a series of simulations of the circuit shown in Fig. 20 with the following parameter values: $L = 18$ mH, $C_2 = 100$ nF, $C_1 = 10$ nF, $G_a = -55/60$ mS $= -757.576\mu$S, $G_b = -9/22$ mS $= -409.091\mu$S, and $E = 1$ V. $R_0 = 12.5\Omega$ models the parasitic series resistance of a real inductor. R is our bifurcation parameter.

Equilibrium Point and Hopf Bifurcation: When R is large (2000 Ω), the outer equilibrium points P_- and P_+ are *stable* ($\gamma_1 < 0$ and $\sigma_1 < 0$, $\omega_1 \neq 0$); the inner equilibrium point 0 is *unstable* ($\gamma_0 > 0$ and $\sigma_0 < 0$, $\omega_0 \neq 0$).

Depending on the initial state of the circuit, the system remains at one outer equilibrium point or the other. Let us assume that we start at P_+ in the D_1 region. This equilibrium point has one negative real eigenvalue and a complex pair with negative real parts. The action of the negative real eigenvalue γ_1 is to squeeze trajectories down onto the complex eigenplane $E^c(P_+)$, where they spiral toward the equilibrium point P_+. Fig. 10(a) shows the geometry of the piecewise-linear vector space when $R = 2000\Omega$ and a trajectory $\mathbf{X}(t)$ that spirals toward the steady-state equilibrium point solution P_+.

As the resistance R is decreased, the real part of the complex pair of eigenvalues changes sign and becomes positive. Correspondingly, the outer equilibrium points become unstable as σ_1 passes through 0; this is called a *Hopf* bifurcation. The real eigenvalue of P_+ remains negative, so trajectories in the D_1 region converge toward the complex eigenplane $E^c(P_+)$. However, they spiral *away* from the equilibrium point P_+ along $E^c(P_+)$ until they reach the dividing plane U_1 (defined by $V_1 \equiv E$) and enter the D_0 region.

The equilibrium point at the origin in the D_0 region has a stable complex pair of eigenvalues and an unstable real

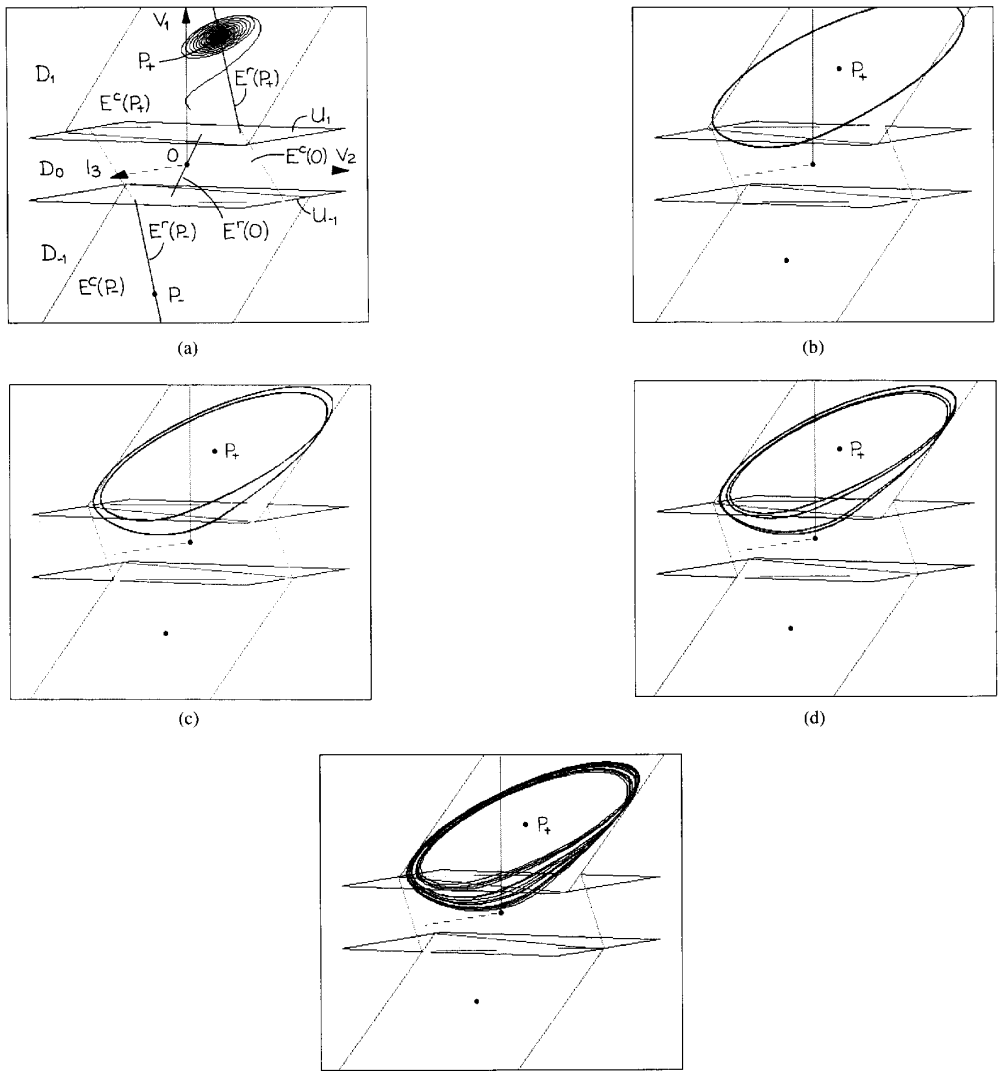

Fig. 10. Simulated period-doubling sequence for Chua's oscillator. (a) $G = 500\mu$S (equilibrium point). P_+ is the equilibrium point in the D_1 region; $E^r(P_+)$ and $E^c(P_+)$ are the corresponding real eigenvector and complex eigenplane respectively. The equilibrium point in the D_0 region is denoted by 0; its real eigenvector is $E^r(0)$ and its complex eigenplane is $E^c(0)$. U_1 is the plane defined by $V_1 = E$ which separates the D_1 and D_0 regions. U_{-1} is the boundary between D_0 and D_{-1}; it is defined by $V_1 = -E$. P_- is the equilibrium point in the D_{-1} region; its complex eigenplane is $E^c(P_-)$ and its real eigenvector is $E^r(P_-)$. (b) $G = 530\mu$S (period-1 limit cycle). The trajectory spirals away from P_+ close to $E^c(P_+)$ until it crosses U_1 and enters D_0, where it is folded back toward D_1. (c) $G = 537\mu$S (period-2 limit cycle); (d) $G = 539\mu$S (period-4 limit cycle); (e) $G = 541\mu$S (Spiral-Chua chaotic attractor).

eigenvalue. Trajectories that enter the D_0 region on the complex eigenplane $E^c(0)$ are attracted to the origin along this plane. Trajectories that enter D_0 from D_1 below or above the eigenplane either cross over to D_{-1} or are turned back toward D_1, respectively. For R sufficiently large, trajectories that spiral away from P_+ along $E^c(P_+)$ and enter D_0 *above* $E^c(0)$ are returned to D_1, producing a stable period 1 *limit cycle*. This is illustrated in Fig. 10(b).

Period-Doubling: As the resistance R is decreased further, a period-doubling or *pitchfork* bifurcation occurs. The limit cycle now closes on itself after encircling P_+ *twice*; this is called a *period 2* cycle because a trajectory takes approximately twice the time to complete this closed orbit as to complete the preceding period 1 orbit (see Fig. 10(c)).

Decreasing the resistance R still further produces a cascade of period-doubling bifurcations to *period 4* (Fig. 10(d)), *period 8*, *period 16*, and so on until an orbit of infinite period is reached, beyond which we have chaos (see Fig. 10(e)). This is a Spiral-Chua *strange attractor*.[5]

The Spiral-Chua attractor in Fig. 10(e) looks like a ribbon or band that is smoothly folded on itself; this folded band

[5]An *attractor* is a *stable* steady-state solution of a dynamical system. An attractor is called *strange* or chaotic if it contains a transversal homoclinic orbit [1].

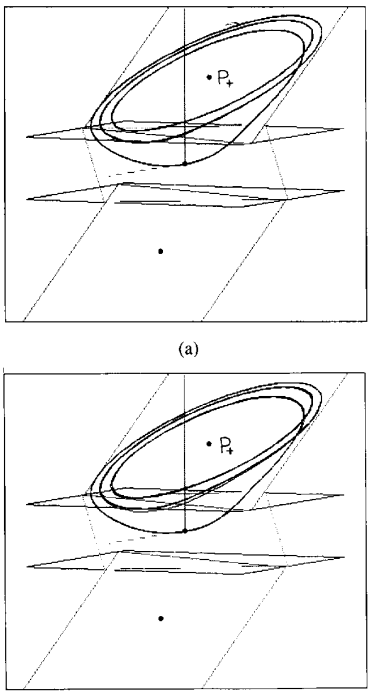

Fig. 11. (a) Simulated period-3 window ($G = 542.5\mu$S) in Chua's oscillator. (b) Period-6 window ($G = 542.8\mu$S).

is the simplest type of strange attractor [12]. A trajectory from an initial condition $\mathbf{X}_0$ winds around the strip repeatedly, returning close to $\mathbf{X}_0$, but never closing on itself.

Periodic Windows: Between the chaotic regions in the parameter space of Chua's circuit, there exist ranges of the bifurcation parameter R over which stable periodic motion occurs. These regions of periodicity are called *periodic windows*. Periodic windows of periods 3 and 5 are readily found in Chua's circuit. These periodic limit cycles undergo period-doubling bifurcations to chaos as the resistance R is decreased. Fig. 11(a) shows a period 3 window, so called because the trajectory encircles the outer equilibrium point P_+ three times before closing on itself. Fig. 11(b) shows a period 6 orbit that results from a period-doubling bifurcation of this period 3 limit cycle.

Spiral-Chua Attractor: Fig. 12 shows three views of another simulated Spiral-Chua strange attractor. Fig. 12(b) is a view along the edge of the outer complex eigenplanes $E^c(P_+)$ and $E^c(P_-)$; notice how trajectories in the D_1 region are compressed toward the complex eigenplane $E^c(P_+)$ along the direction of the stable real eigenvector $E^r(P_+)$ and that they spiral away from the equilibrium point P_+ along $E^c(P_+)$.

When a trajectory enters the D_0 region through U_1 from D_1, it is twisted around the unstable real eigenvector $E^r(0)$ and returned to D_1.

Fig. 12(c) shows clearly that when the trajectory enters D_0 from D_1, it crosses U_1 *above* the eigenplane $E^c(0)$. The trajectory cannot cross through this eigenplane; therefore, it must return to the D_1 region.

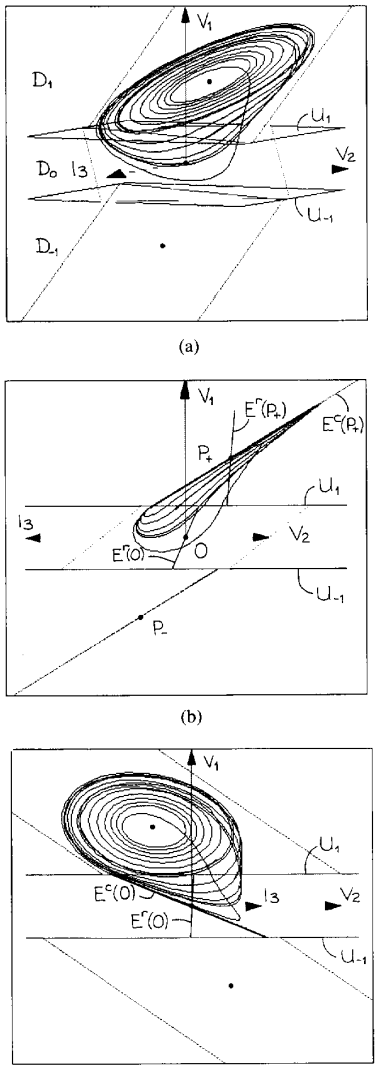

Fig. 12. Three views of a simulated Spiral-Chua attractor in Chua's oscillator with $G = 550\mu$S. (a) Reference view (compare with Figs. 10 and 11). (b) View along the edge of the outer complex eigenplanes $E^c(P_+)$ and $E^c(P_-)$; note how the trajectory in D_1 is flattened onto $E^c(P_+)$. (c) View along the edge of the complex eigenplane $E^c(0)$; trajectories cannot cross this plane.

Double-Scroll Chua Attractor: Because we chose a nonlinear resistor with a symmetric nonlinearity, every attractor that exists in the D_1 and D_0 regions has a counterpart (mirror image) in the D_{-1} and D_0 regions. As the coupling resistance R is decreased further, the Spiral-Chua attractor "collides" with its mirror image, and the two merge to form a single compound attractor called a double-scroll Chua strange attractor [2], as shown in Fig. 13.

Once more, we show three views of this attractor in order to illustrate its geometrical structure. Fig. 13(b) is a view of the attractor along the edge of the outer complex eigenplanes $E^c(P_+)$ and $E^c(P_-)$. Upon entering the D_1 region from D_0, the trajectory collapses onto $E^c(P_+)$ and spirals away from P_+ along this plane.

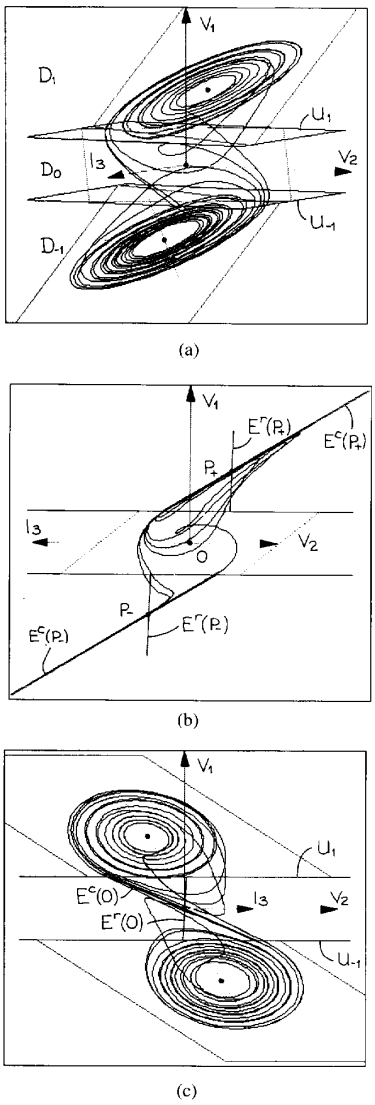

Fig. 13. Three views of a simulated double-scroll Chua attractor in Chua's oscillator with $G = 565\mu$S. (a) Reference view (compare with Figs. 10, 11, and 12). (b) View along the edge of the outer complex eigenplanes $E^c(P_+)$ and $E^c(P_-)$; note how the trajectory in D_1 is flattened onto $E^c(P_+)$ and onto $E^c(P_-)$ in D_{-1}. (c) View along the edge of the complex eigenplane $E^c(0)$; a trajectory entering D_0 from D_1 above this plane returns to D_1 while one entering D_0 below $E^c(0)$ crosses to D_{-1}.

Fig. 13(c) is a view of the attractor along the edge of the complex eigenplane $E^c(0)$ in the inner region. Notice once more that when the trajectory crosses U_1 into D_0 above $E^c(0)$, it must remain above $E^c(0)$ and so returns to D_1. Similarly, if the trajectory crosses U_1 below $E^c(0)$, it must remain below $E^c(0)$ and therefore crosses over to the D_{-1} region. Thus, $E^c(0)$ presents a knife-edge to the trajectory as it crosses U_1 into the D_0 region, forcing it back toward D_1 or across D_0 to D_{-1}.

Boundary Crisis: Reducing the resistance R still further produces more regions of chaos, interspersed with periodic windows. Eventually, for a sufficiently small value of R, the unstable saddle trajectory [2] that normally resides outside the stable steady-state solution collides with the double-scroll Chua attractor, and a *boundary crisis*[13] occurs. After this, all trajectories become unbounded. While an unbounded trajectory can occur in a computer simulation, the real world behaves slightly differently, as we shall see.

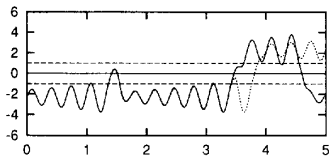

Fig. 14. Sensitive dependence on initial conditions. Two time waveforms $V_1(t)$ from Chua's oscillator with $G = 550\mu$S, starting from (I_3, V_2, V_1) = (1.810mA, 222.014mV, -2.286V) [solid line] and (I_3, V_2, V_1) = (1.810mA, 222.000mV, -2.286V) [dashed line]. Note that the trajectories diverge within 5 ms. Horizontal axis: t (ms); Vertical axis: V_1 (V). Compare with Fig. 13.

Characteristics of Chaos

Sensitive Dependence on Initial Conditions: Consider once more the double-scroll Chua attractor shown in Fig. 13. Two trajectories starting from distinct, but almost identical, initial states in D_1 will remain close together until they reach the separating plane U_1. Imagine that the trajectories are still close at the knife-edge, but that one trajectory crosses into D_0 slightly above $E^c(0)$ and the other slightly below $E^c(0)$. The former trajectory returns to D_1, and the latter crosses over to D_{-1}; their "closeness" is lost.

The time-domain waveforms $V_1(t)$ for two such trajectories are shown in Fig. 14. These are solutions of Chua's oscillator with the same parameters as those in Fig. 13; the initial conditions are (I_3, V_2, V_1) = (1.810mA, 222.014mV, -2.286V) (solid line) and (I_3, V_2, V_1) = (1.810mA, 222.000mV, -2.286V) (dashed line). Although the initial conditions differ by less than 0.01% in just one component (V_2), the trajectories diverge and become uncorrelated within 5 ms because one crosses the knife-edge before the other.

This rapid decorrelation of trajectories that originate in nearby initial states, commonly called *sensitive dependence on initial conditions*, is a generic property of chaotic systems. It gives rise to an apparent *randomness* in the output of the system and long-term unpredictability of the state.

Because chaotic systems are *deterministic*, two trajectories that start from *identical* initial states will follow precisely the same paths through the state space. In practice, it is impossible to construct two systems with identical parameters, let alone to start them from identical initial states. However, recent work by Pecora and Carroll and others [14], [15] has shown that it is possible to *synchronize* two chaotic systems so that their trajectories remain close. These ideas are now being exploited in secure communication systems. Information modulated onto a "random" chaotic carrier can be demodulated by using a synchronized receiver (see, e.g., [16]–[18]).

Randomness in the Time Domain: Fig. 15(a), 15(b) , and 15(c) show the voltage waveforms $V_1(t)$ corresponding to the period 1, period 2, and Spiral-Chua attractors in Figs. 10(b), 10(c), and 12, respectively. The period 1 waveform is

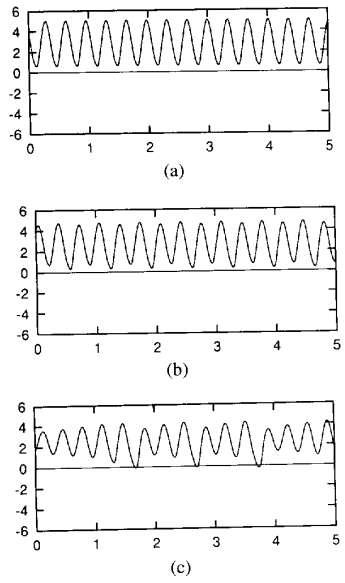

Fig. 15. Simulated time waveforms $V_1(t)$ from Chua's oscillator with (a) $G = 530\mu$S (period 1 limit cycle); (d) $G = 537\mu$S (period 2 limit cycle); (c) $G = 550\mu$S (Spiral-Chua chaotic attractor). Horizontal axis: t (ms); Vertical axis: V_1 (V). Compare with Figs. 10(b), 10(c), and 12, respectively.

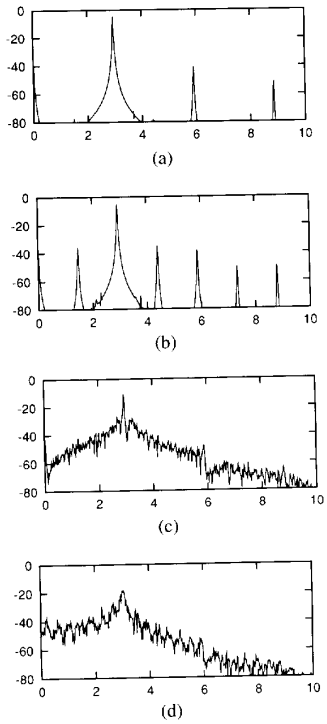

Fig. 16. Power spectra for simulated time waveforms $V_2(t)$ from Chua's oscillator with (a) $G = 530\mu$S (period-1 limit cycle)—the power spectrum consists of a fundamental frequency and higher harmonics; (d) $G = 537\mu$S (period-2 limit cycle)—this periodic signal is characterized by a discrete power spectrum; (c) $G = 550\mu$S (Spiral-Chua chaotic attractor)—a chaotic waveform has a broadband power spectrum; (d) $G = 565\mu$S (double-scroll Chua chaotic attractor). Horizontal axis: frequency (kHz); Vertical axis: power (mean squared amplitude of $V_2(t)$) (dB).

periodic; it looks like a slightly distorted sinusoid. The period 2 waveform is also periodic. It differs qualitatively from the period 1 in that the pattern of a large peak followed by a small peak repeats approximately once every *two* cycles of the period 1 signal; this is why it is called period 2.

In contrast to these periodic time waveforms, $V_1(t)$ for the Spiral-Chua strange attractor is quite irregular and does not appear to repeat itself in any observation period of finite length. Although it is produced by a third-order *deterministic* differential equation, the solution looks "random."

Broadband Power Spectrum: Every periodic signal may be decomposed into a Fourier series—a weighted sum of sinusoids at integer multiples of a fundamental frequency [19]. Thus, a periodic signal appears in the frequency domain as a set of spikes at the fundamental frequency and its harmonics. The amplitudes of these spikes correspond to the coefficients in the Fourier series expansion. The Fourier transform is an extension of these ideas to aperiodic signals; one considers the distribution of the signal's power over a continuum of frequencies rather than on a discrete set of harmonics [19], [20].

The distribution of power in a signal $x(t)$ is most commonly quantified by means of the *power density spectrum*, often simply called the *power spectrum*. The simplest estimator of the power spectrum is the periodogram [20], [21], which, given N uniformly spaced samples $x(m/f_s), m = 0, 1, \ldots, N-1$ of $x(t)$, yields $N/2 + 1$ numbers $P(nf_s/N), n = 0, 1, \ldots, N/2$, where f_s is the sampling frequency.

If one considers the signal $x(t)$ as being composed of sinusoidal components at discrete frequencies, then $P(nf_s/N)$ is an estimate of the power in the component at frequency nf_s/N. By Parseval's theorem, the sum of the power in each of these components equals the mean-squared amplitude of the N samples of $x(t)$ [21], [22].

If $x(t)$ is *periodic*, then its power will be concentrated in a dc component, a fundamental frequency component, and harmonics. In practice, the discrete nature of the sampling process causes power to "leak" between adjacent frequency components; this leakage may be reduced by "windowing" the measured data before calculating the periodogram [20], [21]. In the following discussion, we consider 8192 samples of $V_2(t)$ recorded at 200 kHz; leakage is controlled by applying a Welch window [21] to the data.

We remarked earlier that the period 1 time waveform corresponding to the attractor in Fig. 10(b), is almost sinusoidal; we expect, therefore, that most of its power should be concentrated at the fundamental frequency. The power spectrum of the period 1 waveform $V_2(t)$ shown in Fig. 16(a) consists of a sharp spike at approximately 3 kHz and higher harmonic components that are over 30 dB less than the fundamental.

Because the period-2 waveform repeats roughly once every 0.67 ms, this periodic signal has a fundamental frequency component at approximately 1.5 kHz (see Fig. 16(b)). Notice, however, that most of the *power* in the signal is concentrated close to 3 kHz.

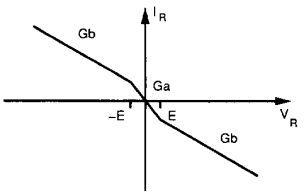

Fig. 17. Required three-segment piecewise-linear DP characteristic for the Chua diode in Fig. 2.

The Spiral–Chua attractor is qualitatively different from these periodic signals. The aperiodic nature of its time-domain waveforms is reflected in the broadband noise-like power spectrum (Fig. 16(c)). No longer is the power of the signal concentrated in a small number of frequency components; rather, it is distributed over a broad range of frequencies. This broadband structure of the power spectrum persists even if the spectral resolution is increased by sampling at a higher frequency f_s.

The chaotic time waveform due to motion on the double-scroll Chua strange attractor also possesses a broad noiselike power spectrum, as shown in Fig. 16(d).

Laboratory Experiment: Chua's Circuit

In this experiment, we demonstrate the concepts of *multiple equilibria, bistability, limit cycles*, and *chaos*. We examine *Hopf* and *period-doubling bifurcations, eventual passivity*, and a *boundary crisis*.

Practical Realization of Chua's Circuit: Chua's circuit can be realized in a variety of ways by using standard or custom-made electronic components. Since all of the linear elements (capacitor, resistor, and inductor) are readily available as two-terminal devices, our principal concern here is with circuitry to realize a nonlinear resistor N_R with the prescribed DP characteristic (shown in Fig. 17).

This line of research was initiated in the mid-1960s, when Chua developed a theory of nonlinear circuit synthesis and realized that such a theory would be academic unless one were allowed to use two-terminal nonlinear resistors with *any* prescribed *v-i* characteristics. This in turn motivated the development of systematic synthesis procedures for two-terminal nonlinear resistors [23], [24], [25], [26], [27], [28]. The term *Chua diode* [29] will henceforth be used to denote any two-terminal nonlinear resistor with a piecewise-continuous DP characteristic synthesized by using standard circuit elements.

Several implementations of Chua diodes with three-segment odd-symmetric piecewise-linear DP characteristics already exist in the literature; these use operational amplifiers (op amps) [7], diodes [6], and transistors. A systematic procedure for synthesizing *precision* piecewise-linear Chua diodes with independently adjustable slopes and breakpoints is described in [30]. Recently, a single-chip integrated circuit (IC) realization of a Chua diode using operational transconductance amplifiers has been reported [31], [32] and an *entire* monolithic Chua's circuit has been fabricated [33].

In this section, we describe a practical implementation of Chua's circuit that uses two op amps and six resistors to implement the Chua diode [29]. This robust circuit is intended for demonstration, research, and educational purposes. While it may appear more complicated than earlier implementations in that the nonlinear resistor comprises two op amps, it is possible to buy two op amps in a single package. Thus, our circuit uses a minimum number of discrete components: a pair of op amps and six resistors to implement the Chua diode, two capacitors, an inductor, and a variable resistor.

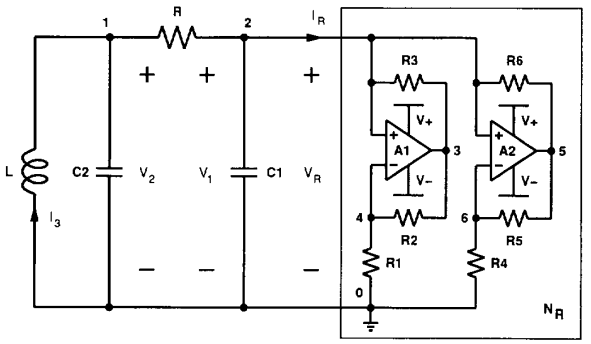

Fig. 18. Practical implementation of Chua's circuit using two op amps and six resistors to realize the Chua diode [29]. Component values are listed in Table I.

TABLE I
COMPONENT LIST FOR THE CIRCUITS USED IN PARTS I AND II OF THIS PAPER

Element	Description	Value	Tolerance
A_1	Op amp ($\frac{1}{2}$ AD712, TL082, or equivalent)		
A_2	Op amp ($\frac{1}{2}$ AD712, TL082, or equivalent)		
C_1	Capacitor	10 nF	±5%
C_2	Capacitor	100 nF	±5%
R	Potentiometer	2 kΩ	
R_1	$\frac{1}{4}$W Resistor	3.3 kΩ	±5%
R_2	$\frac{1}{4}$W Resistor	22 kΩ	±5%
R_3	$\frac{1}{4}$W Resistor	22 kΩ	±5%
R_4	$\frac{1}{4}$W Resistor	2.2 kΩ	±5%
R_5	$\frac{1}{4}$W Resistor	220 Ω	±5%
R_6	$\frac{1}{4}$W Resistor	220 Ω	±5%
L	Inductor (TOKO type 10RB or equivalent)	18 mH	±10%

Circuit Description: Fig. 18 shows a practical implementation of Chua's circuit using a dual op amp and six resistors to implement the Chua diode N_R. A complete list of components is given in Table I.

In addition to the components listed, we recommend that two bypass capacitors of at least $0.1\mu F$ each should be connected between the power supplies and ground, as close to the op amps as possible. The purpose of these capacitors is to maintain the power supplies at a steady dc voltage.

The op amp subcircuit consisting of A_1, A_2 and R_1–R_6 functions as a nonlinear resistor N_R with driving-point characteristic as shown in Fig. 19. Using two 9V batteries to power the op amps gives $V^+ = 9V$ and $V^- = -9V$. From measurements of the saturation levels of the AD712 outputs, $E_{sat} \approx 8.3V$, giving $E \approx 1$V. With $R_2 = R_3$ and

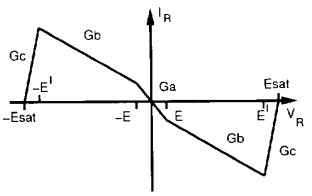

Fig. 19. Every physically realizable nonlinear resistor N_R is eventually passive—the outermost segments (while not necessarily linear as shown here) must lie completely within the first and third quadrants of the V_R–I_R plane for sufficiently large $|V_R|$ and $|I_R|$.

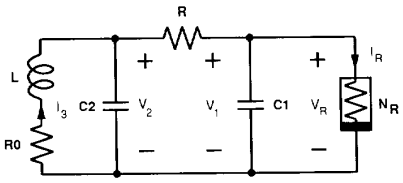

Fig. 20. Equivalent circuit of the practical realization of Chua's circuit shown in Fig. 18. The DP characteristic of the Chua diode is as shown in Fig. 19.

$R_5 = R_6$, the nonlinear characteristic is defined by $G_a = -1/R_1 - 1/R_4 = -50/66$ mS, $G_b = 1/R_3 - 1/R_4 = -9/22$ mS, and $E = R_1 E_{sat}/(R_1 + R_2) \approx 1$ V [29].

Eventual Passivity and the Outer Dissipative Segments: The DP characteristic of the op amp-based Chua diode differs from the desired piecewise-linear characteristic shown in Fig. 17 in that it has *five* segments, the outer two of which have positive slopes $G_c = 1/R_5 = 1/220$s. Every physical resistor is *eventually passive*, meaning simply that for a large enough voltage across its terminals, the instantaneous power $p(t)$ $(= v(t)i(t))$ consumed by a real resistor is positive. For large enough $|v|$ or $|i|$, therefore, its DP characteristic must lie only in the first and third quadrants of the v–i plane. Hence, the DP characteristic of a real Chua diode must include at least two outer segments with positive slopes which return the characteristic to the first and third quadrants (see Fig. 19). From a practical point of view, as long as the voltages and currents on the attractor are restricted to the negative resistance region of the characteristic, these outer segments will not affect the circuit's behavior.

By definition, every attractor is bounded. Therefore, it is always possible to scale the voltages and currents in the circuit so that any particular steady-state solution lies completely within the inner three segments of the Chua diode's DP characteristic (see [29] and [30], for example).

The simplified equivalent circuit of Fig. 18 is shown in Fig. 20. We model the real inductor as a series connection of an ideal linear inductor L and a linear resistor R_0.

Experimental Verification of a Voltage-Controlled DP Characteristic: The DP characteristic of the nonlinear resistor N_R can be measured in isolation by means of the circuit shown in Fig 21.

Resistor R_S, known as a current-sensing resistor, is used to measure the current I_R which flows into the nonlinear resistor N_R when a voltage V_R is applied across its terminals. An appropriate choice of R_S in this example is 100 Ω. Current

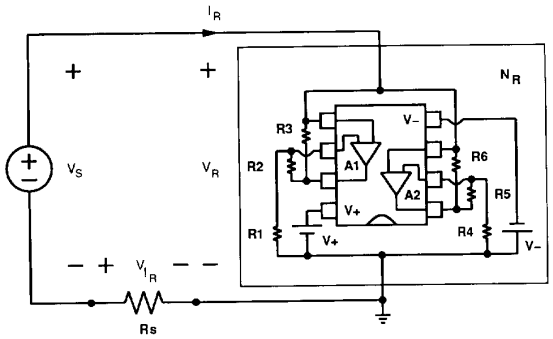

Fig. 21. The DP characteristic of Chua diode N_R can be measured by applying a triangular voltage waveform V_S to the series combination of N_R and a small current-sensing resistor R_S. Plot $-V_{I_R}(\propto I_R)$ versus V_R. The eight-pin dual op amp package is shown from above in schematic form. The reference end of the package is indicated by a dot or a semicircle (shown here).

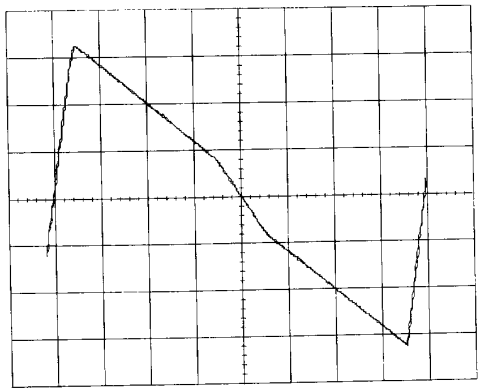

Fig. 22. Measured v–i characteristic of the Chua diode in Fig. 18. V_S is a triangular waveform with zero DC offset, amplitude 15V peak-to-peak, and frequency 30 Hz. Horizontal axis: V_R (2V/div); Vertical axis: $-V_{I_R}$ (100mV/div).

I_R flowing in R_S then causes a voltage $V_{I_R} = -100 I_R$ to appear across the sensing resistor. Thus, we can measure the DP characteristic of N_R by applying a voltage V_S as shown and plotting $V_{I_R}(\propto -I_R)$ versus V_R. This is achieved by connecting V_{I_R} to the y-input and V_R to the x-input of an oscilloscope in x-y mode. The resulting characteristic for the components listed in the table is shown in Fig 22. Note that we have plotted $-V_{I_R}$ versus V_R; this is possible if your oscilloscope permits inversion of the y-input in x-y mode.

Practical Considerations for Op-Amp Based Chua Diodes: The breakpoints in the Chua diode's DP characteristic are proportional to the saturation levels of the op amps. The saturation levels in turn are determined by the power supply voltages and by the internal architecture of the op amps. If the levels are different, as they typically are, the resulting DP characteristic will be asymmetric. This results in a double-scroll Chua attractor which has one lobe bigger than the other.

Furthermore, the input offset voltage of an op amp causes a shift in the DP characteristic when it is used to implement a

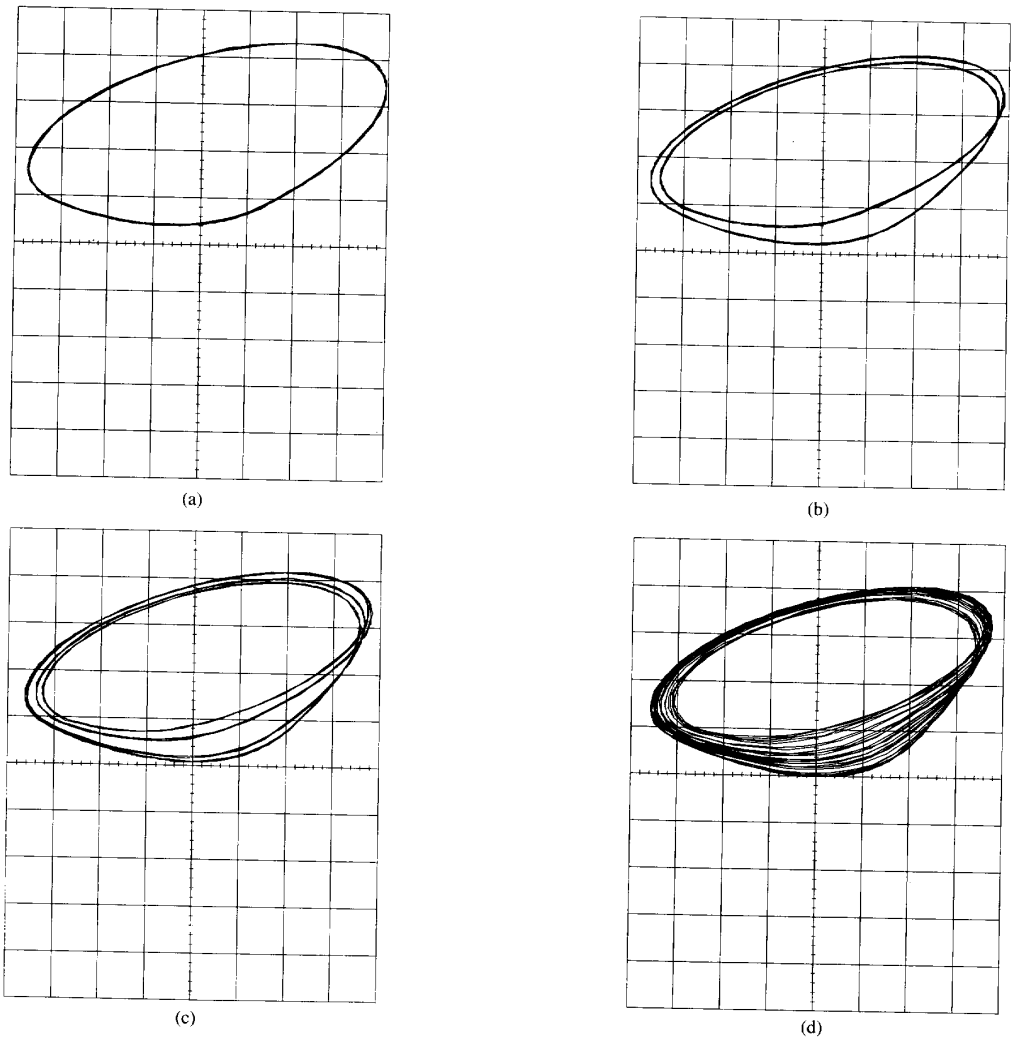

Fig. 23. Typical experimental bifurcation sequence in Chua's circuit (component values as in Table I) recorded by using a Hitachi VC-6025 Digital Storage Oscilloscope. Horizontal axis V_2 (a)–(h) 200mV/div, (i) 2V/div; vertical axis V_1 (a)–(h) 1V/div, (i) 2V/div. (a) $R = 1.83k\Omega$, period 1; (b) $R = 1.82k\Omega$, period 2; (c) $R = 1.81k\Omega$, period 4; (d) $R = 1.80k\Omega$, Spiral–Chua attractor.

Chua diode. While asymmetry may be aesthetically unpleasing, it has little effect on the bifurcation sequence or on the nature of the attractor.

If one wishes, the asymmetry due to saturation level mismatch may be corrected by adjusting the positive and negative power supply voltages until symmetry is achieved. For example, the negative saturation level might be 0.7 V less in magnitude than the positive level. This could be corrected by using power supplies of 9 V and -9.7 V instead of ± 9 V.

Normally, it is not possible to zero the offset in an 8-pin dual op amp such as the AD712 or the TL082. In fact, we deliberately chose the AD712 because it draws negligible input current, by virtue of its FET input stage, and has a guaranteed maximum input offset voltage of 1.0 mV (AD712K) [34]. If the offset is disturbing, one may substitute for the dual op amp two single op amp equivalents such as the AD711 and TL081; these have offset balancing pins to enable the user to zero the offset voltage.

Steady-State Solutions: A 2-D projection of each steady-state solution may be obtained by connecting V_2 and V_1 to the X and Y channels, respectively, of an X-Y oscilloscope.

Bifurcations and Chaos: By reducing the variable resistor R in Fig. 18 from 2000 Ω toward zero, Chua's circuit exhibits a Hopf bifurcation from dc equilibrium, a sequence of period-doubling bifurcations to a Spiral–Chua attractor, periodic windows, double-scroll Chua strange attractor, and a boundary crisis, as illustrated in Fig. 23.

Notice that varying R in this way causes the size of the attractors to change: the period 1 orbit is large; period 2 is smaller; the Spiral-Chua attractor is smaller again; and the double-scroll Chua attractor shrinks considerably before it dies. This shrinking is due to the equilibrium points P_+ and

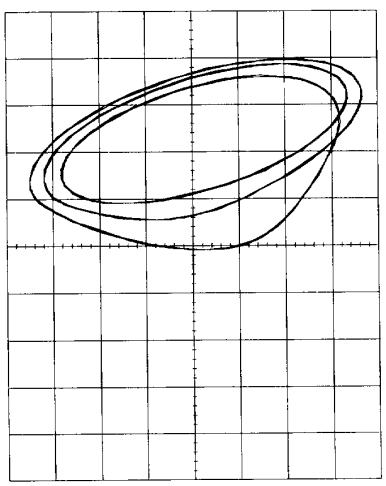

(e)

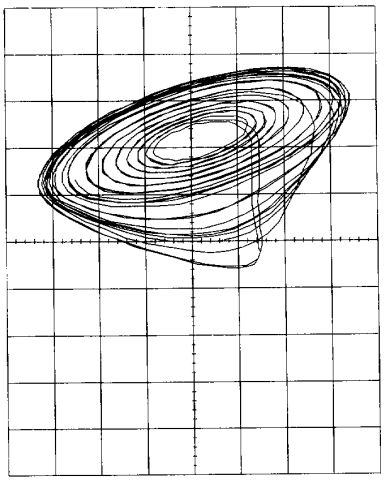

(f)

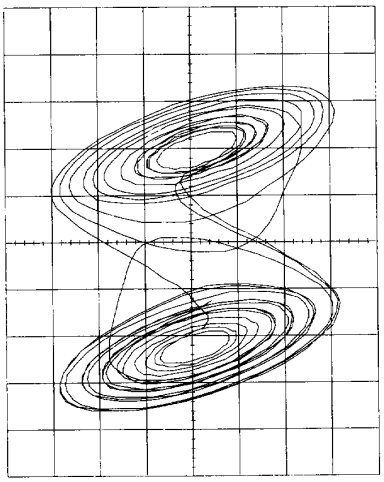

(g)

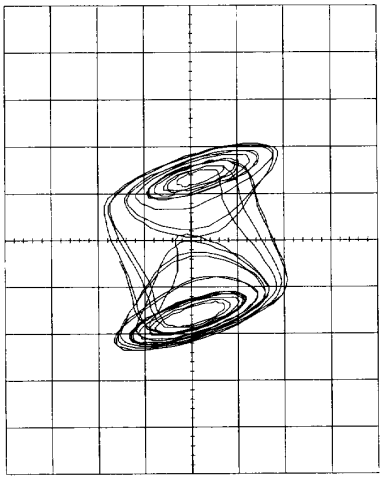

(h)

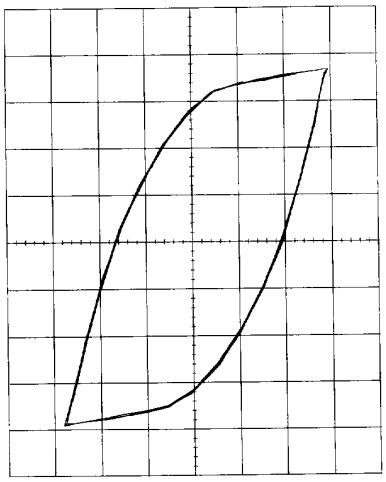

(i)

Fig. 23 (*continued*). (e) $R = 1.797k\Omega$, period 3 window; (f) $R = 1.76k\Omega$, Spiral–Chua attractor; (g) $R = 1.73k\Omega$, double-scroll Chua attractor; (h) $R = 1.52k\Omega$, double-scroll Chua attractor; (i) $R = 1.42k\Omega$, large limit cycle corresponding to the outer segments of the Chua diode's DP characteristic.

P_- moving closer to the origin as R is decreased. This is easier to see in the simulations. Compare the position of P_+ in Figs. 10(a) and 13.

Alternative Bifurcation Sequence: An alternative way to view a bifurcation sequence is by adjusting C_1. Fix the value of R at 1800 Ω and vary C_1; monitor V_1 and V_2 as before. The full range of dynamical behaviors from equilibrium through Hopf, and period-doubling bifurcations, periodic windows, Spiral-Chua and double-scroll Chua chaotic attractors can be observed as C_1 is reduced from 12.0 nF to 6.0 nF. Unlike the R bifurcation sequence, the size of the double-scroll attractor remains almost constant in the C_1 bifurcation sequence because the *positions* of the equilibrium points are independent of C_1.

Eventual Passivity and the Big Limit Cycle: We noted earlier that no physical system can have unbounded trajectories; in particular, any physical realization of a Chua diode is *eventually passive*. The "unbounded" trajectories that follow the boundary crisis are thus limited in amplitude by the power supplies that are used to power the Chua diode, and a large limit cycle results as shown in Fig. 23(i). This effect could of course be simulated by using a five-segment DP characteristic for N_R as shown in Fig. 19.

Simulation of Chua's Circuit

Our experimental observations and qualitative description of the global dynamics of Chua's circuit may be confirmed by simulation using a specialized Nonlinear Dynamics simulation package such as INSITE [35], [36], or by employing a customized simulator. All of the computer-generated figures so far in Parts I and II of this tutorial paper were produced by using special-purpose software called "Adventures in Bifurcations and Chaos" (ABC), which was developed specifically to accompany this work. The program (which uses a fourth-order Runge-Kutta integration routine [35]) is written in Microsoft QuickBASIC and runs without compilation on every IBM-compatible computer that has the MS-DOS version 5.0 operating system.

"ABC" simulates three example circuits: the linear and nonlinear parallel RLC circuits described in Part I, and Chua's oscillator. For the two-dimensional examples, it generates and plots vector fields, time waveforms, and trajectories. In the case of Chua's oscillator, the program calculates and draws equilibrium points, eigenvalues, eigenspaces, and trajectories. A two-dimensional projection of the three-dimensional dynamics is shown in a state space plot, and the corresponding time waveforms are simultaneously displayed in a time-domain window. The user may change the parameters, initial condition, and viewing angle, as illustrated in Fig. 13. The ability to view the attractor in a variety of orientations, and thus to "walk through" the three-dimensional state space, permits one to visualize readily the geometric structure of the dynamics.

In addition, the software is accompanied by an extensive database of sets of initial conditions and parameters that produce every dynamical behavior that has been reported for Chua's oscillator: equilibrium points, bifurcation sequences, periodic orbits, homoclinic and heteroclinic orbits [1], and a plethora of chaotic attractors [8]. This library of steady-state solutions has been prepared over several years in collaboration with Leon Chua's research group at the University of California at Berkeley. It will be maintained and extended as new attractors are discovered.[6]

SPICE Simulations

For electrical engineers who are familiar with the SPICE circuit simulator [37], but perhaps not with chaos, we present a net-list and simulation results for our robust implementation of Chua's circuit. The AD712 op amps in this realization of the circuit are modeled using Analog Devices' AD712 macromodel [38]. The TOKO 10RB inductor has a nonzero series resistance which we have included in the SPICE net-list; we measured `R0` = 12.5Ω. Node numbers are the same as those in Fig. 18: the power rails are 111 and 222; 10 is the "internal" node of our physical inductor where its series inductance is connected to its series resistance.

A double-scroll Chua attractor results from our SPICE 3e2 simulation using the input deck shown in Fig. 24. This attractor is plotted in Fig. 25.

Dimensionless Coordinates and the α–β Bifurcation Diagram: Thus far, we have discussed Chua's circuit equations in terms of seven parameters L, C_2, G, C_1, E, G_a, and G_b. We can reduce the number of parameters by normalizing the nonlinear resistor such that its breakpoints are at ± 1V instead of $\pm E$V. Furthermore, we may write Chua's circuit equations (2)–(4) in *normalized dimensionless form* by making the following change of variables: $x = V_1/E$, $y = V_2/E$, $z = I_3/(EG)$, and $\tau = tG/C_2$. Thus:

$$\frac{dz}{d\tau} = -\beta y \tag{8}$$

$$\frac{dy}{d\tau} = x - y + z \tag{9}$$

$$\frac{dx}{d\tau} = \alpha(y - h(x)) = \begin{cases} \alpha(y - bx - (b-a)) & \text{if} \quad x < -1 \\ \alpha(y - ax) & \text{if} \quad -1 \le x \le 1 \\ \alpha(y - bx - (a-b)) & \text{if} \quad x > 1 \end{cases} \tag{10}$$

where $a = G_a'/G = 1 + G_a/G$, $b = G_b'/G = 1 + G_b/G$, $\alpha = C_2/C_1$, and $\beta = C_2/(LG^2)$. Thus, each set of seven circuit parameters has an equivalent set of four normalized dimensionless parameters $\{a, b, \alpha, \beta\}$. If we fix the values of a and b (which correspond to the slopes G_a and G_b of the Chua diode), we can summarize the steady-state dynamical behavior of Chua's circuit by means of a *two-dimensional* α–β diagram.

Fig. 26 shows the two-parameter bifurcation diagram in the (α, β)–plane with $a = -1/7$ and $b = 2/7$. In this diagram, each colored region denotes a particular type of steady-state behavior: for example, an equilibrium point, period 1, trajectory, period 2, Spiral–Chua attractor, double-scroll Chua attractor. Typical state-space behaviors are shown in the insets. For clarity, we show chaotic regions in a single color; it should

[6]Contact the author (e-mail address: mpk@midir.ucd.ie) for a free copy of "ABC."

```
ROBUST OP AMP REALIZATION OF CHUA'S CIRCUIT

V+  111 0   DC 9
V-  0   222 DC 9
L   1  10   0.018
R0  10 0    12.5
R   1  2    1770
C2  1  0    100.0N
C1  2  0    10.0N
XA1  2 4 111 222 3 AD712
R1   2 3  220
R2   3 4  220
R3   4 0  2200
XA2  2 6 111 222 5 AD712
R4   2 5  22000
R5   5 6  22000
R6   6 0  3300

* AD712 SPICE Macro-model       1/91, Rev. A
* Copyright 1991 by Analog Devices, Inc. (reproduced with permission)
*
.SUBCKT AD712 13 15 12 16 14
*
VOS 15 8 DC 0
EC 9 0 14 0 1
C1 6 7 .5P
RP 16 12 12K
GB 11 0 3 0 1.67K
RD1 6 16 16K
RD2 7 16 16K
ISS 12 1 DC 100U
CCI 3 11 150P
GCM 0 3  0 1  1.76N
GA 3 0  7 6  2.3M
RE 1 0 2.5MEG
RGM 3 0 1.69K
VC 12 2 DC 2.8
VE 10 16 DC 2.8
RO1 11 14 25
CE 1 0 2P
RO2 0 11 30
RS1 1 4 5.77K
RS2 1 5 5.77K
J1 6 13 4 FET
J2 7 8 5 FET
DC 14 2 DIODE
DE 10 14 DIODE
DP 16 12 DIODE
D1 9 11 DIODE
D2 11 9 DIODE
IOS 15 13 5E-12
.MODEL DIODE D
.MODEL FET PJF(VTO=-1 BETA=1M IS=25E-12)
.ENDS

.IC V(2)=0.1 V(1)=0
.TRAN 0.1MS 75.0MS 50.0MS
.PRINT TRAN V(2) V(1)
.PLOT TRAN V(2) V(1)
.END
```

Fig. 24. SPICE deck to simulate the transient response of our dual op amp implementation of Chua's circuit. Node numbers are the same as those in Fig. 10. The op amps are modeled by the Analog Devices AD712 macro model. R0 models the series resistance of the real inductor L.

be noted that these chaotic regions are further partitioned by periodic windows and "islands" of periodic behavior.

To interpret the α–β diagram, imagine fixing the value of $\beta = C_2/(LG^2)$ and increasing $\alpha = C_2/C_1$ from a positive value to the left of the curve labeled "Hopf at $P^{\pm}$"; experimentally, this corresponds to fixing the parameters L, C_2, G, E, G_a, and G_b, and reducing the value of C_1 (previously, we called this a "C_1 bifurcation sequence").

Initially, the steady-state solution is an equilibrium point. As the value of C_1 is reduced, the circuit undergoes a Hopf bifurcation when α crosses the "Hopf at $P^{\pm}$" curve. Decreasing C_1 still further, the steady-state behavior bifurcates from period 1 to period 2 to period 4 and so on to chaos, periodic windows, and a double-scroll Chua attractor. The right edge of the chaotic region is delimited by a curve corresponding to the boundary crisis and "death" of the attractor. Beyond this curve, trajectories diverge toward infinity. Because of eventual passivity in a real circuit, these divergent trajectories will of course converge to a limit cycle in any physical implementation of Chua's circuit.

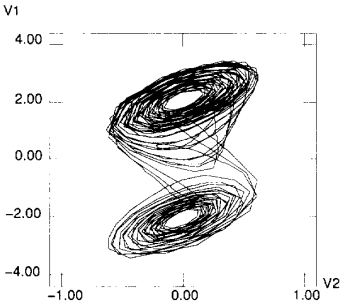

Fig. 25. SPICE 3e2 simulation of Fig. 18 using the input deck shown in Fig. 24 yields this double-scroll Chua attractor. Horizontal axis V_2 (V); vertical axis V_1 (V). The jaggedness of the trajectory results from the large timestep chosen by SPICE's integration routine when using its default accuracy settings.

Reality of Chaos

We saw earlier that a chaotic system is characterized by sensitive dependence on initial conditions: Small perturbations of the state grow exponentially with time. The approximation involved in integrating Chua's circuit equations numerically and the effects of small random perturbations due to noise in an experiment produce simulated and experimental trajectories of chaotic systems that are *not* exact solutions of the state equations.[7] It follows that any claim that a system is chaotic can be made only if accompanied by a rigorous mathematical proof.

In general, it is extremely difficult to prove the existence of chaos in continuous-time systems. However, such a proof has been given for Chua's circuit by Chua *et al.* [2]. We paraphrase this result as follows:

Theorem—Mathematical Chaos in Chua's Circuit: There exist regions in the (α, β) parameter space where the motion on a double-scroll Chua attractor is technically equivalent to that generated by a mathematical model of a coin toss–the Bernouilli shift.

This theorem provides the first rigorous proof of chaos (in the sense of Shilnikov) for a *physical* system whose theoretical behavior agrees with both computer simulations and experimental results.

III. Concluding Remarks

In this two-part tutorial paper, we have guided the reader into the exciting world of nonlinear dynamics in continuous systems. By means of guided examples and experiments, we have studied the concepts of steady-state solutions, equilibrium points, stability, bifurcations, local and global dynamics, limit cycles, and chaos.

In Part I, we showed that while the familiar linear parallel RLC circuit is a poor model of sustained oscillation in real systems, it is a useful aid in developing insights into the nature

[7] Nevertheless, computed and observed trajectories do lie close to the underlying strange attractor if the local integration error or experimental noise is small [36].

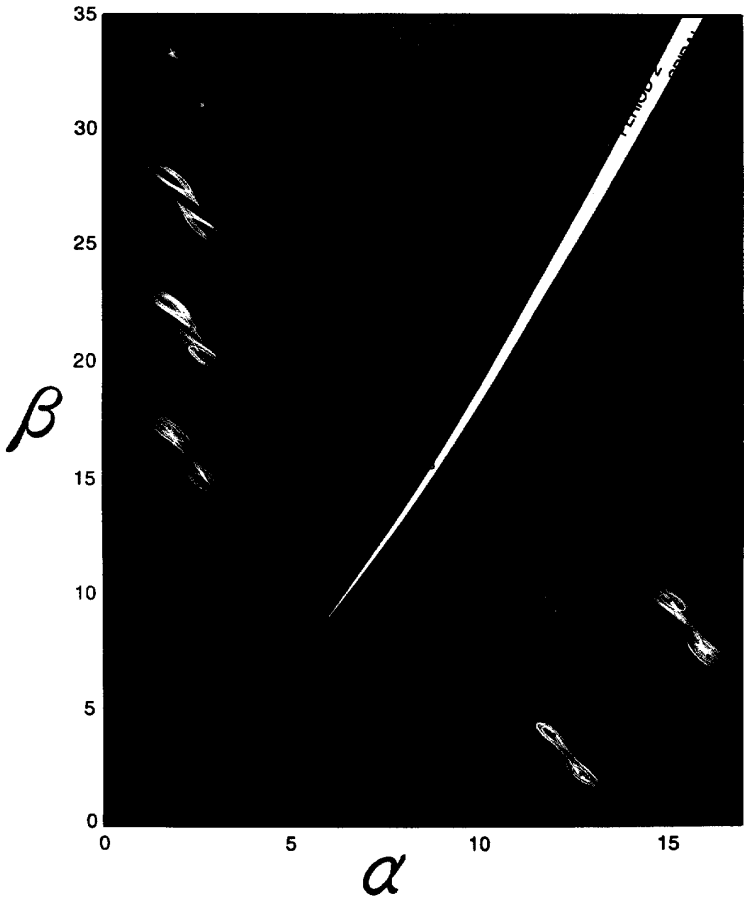

Fig. 26. Two-parameter α–β bifurcation diagram for the normalized dimensionless Chua's circuit equations (8)–(10) with $a = -1/7$ and $b = 2/7$.

of oscillation. Using the framework of piecewise-linear circuit theory, we showed how the linear RLC circuit could be used to explain the local behavior of more complicated systems. In particular, we inserted a series voltage-controlled nonlinear resistor in the parallel RLC circuit and saw how this forced us to add an additional transit capacitor to the circuit in order that it be well defined. In this way, the linear parallel RLC resonant circuit evolved into Chua's circuit.

In Part II, we have used the tools and insights developed in Part I to explain the geometrical origins of complex dynamics and chaos in Chua's circuit. We have supported these qualitative observations with computer simulations and experiments.

Chaos is characterized by a stretching and folding mechanism. Nearby trajectories of a deterministic dynamical system are pulled apart and folded back together repeatedly to produce complicated bounded nonperiodic motion on a strange attractor. The exponential divergence of trajectories that underlies chaotic behavior, and the resulting sensitivity to initial conditions, lead to long-term unpredictability which manifests itself as randomness in the time-domain and produces a broadband noiselike power spectrum.

While differential equations and mechanical systems provide convenient frameworks in which to examine bifurcations and chaos, electronic circuits are unique in being easy to build, easy to measure, and easy to model. Furthermore, they operate in real time, and parameter values are readily adjusted. Just as the linear parallel RLC resonant circuit is the simplest paradigm for understanding *periodic* steady-state phenomena in linear circuits, so Chua's circuit presents an attractive paradigm for studying *nonperiodic* phenomena in nonlinear circuits. The importance of Chua's circuit and its relatives [39], [40], [41], [42], [43] is that they can exhibit *every* type of bifurcation and attractor that has been reported to date in third-order continuous-time dynamical systems. While exhibiting a rich variety of complex dynamical behaviors, the circuit is simple enough to be constructed and modeled by using standard electronic parts and simulators.

We strongly encourage the reader to simulate, build, and analyze the circuits that we have presented here as aids to understanding the nature of oscillation and complex dynamics.

ACKNOWLEDGMENT

I am grateful to Prof. L. Chua (University of California at Berkeley) for his support and encouragement, Mr. C. Wu (University of California at Berkeley) for adding the Chua oscillator database to ABC, Prof. J. G. Lacy (University

College Dublin) for allowing me to use his computers, Mr. B. Mulkeen (University College Dublin) for introducing me to compiled QuickBASIC, Dr. P. Curran (University College Dublin) for stimulating discussions on ODE's and chaos, Prof. M. Ogorzalek and Prof. L. Kocarev for their constructive criticism, and Mr. D. Sheingold (Analog Devices) for efficiently processing my request for permission to reproduce the AD712 macro-model.

REFERENCES

[1] J. Guckenheimer and P. Holmes, *Nonlinear Oscillations, Dynamical Systems, and Bifurcations of Vector Fields*. New York: Springer-Verlag, 1983.
[2] L. O. Chua, M. Komuro, and T. Matsumoto, "The double scroll family, Parts I and II," *IEEE Trans. Circuits Syst.*, vol. CAS-33, no. 11, pp. 1073–1118, 1986.
[3] A. I. Mees and P. B. Chapman, "Homoclinic and heteroclinic orbits in the double scroll attractor," *IEEE Trans. Circuits Syst.*, vol. CAS-34, no. 9, pp. 1115–1120, 1987.
[4] M. J. Ogorzalek, "Taming chaos: Part II—Control," *IEEE Trans. Circuits Syst.*, this issue.
[5] L. O. Chua, C. A. Desoer, and E. S. Kuh, *Linear and Nonlinear Circuits*. New York: McGraw-Hill, 1987.
[6] T. Matsumoto, "A chaotic attractor from Chua's circuit," *IEEE Trans. Circuits Syst.*, vol. CAS-31, vol. 12, pp. 1055–1058, 1984.
[7] G. Q. Zhong and F. Ayrom, "Experimental confirmation of chaos from Chua's circuit," *Int. J. Circuit Theory Appl.*, vol. 13, no. 11, pp. 93–98, 1985.
[8] L. O. Chua, "Global unfolding of Chua's circuit," *IEICE Trans. Fundamentals (Special Issue on Chaos, Neural Networks, and Numerics)*, vol. E76-A, no. 5, pp. 704–734, May 1993.
[9] ——, "The genesis of Chua's circuit," *Archiv für Elektronik und Übertragungstechnik*, vol. 46, no. 4, pp. 250–257, 1992.
[10] V. I. Arnold, *Ordinary Differential Equations*. Cambridge, MA: MIT Press, 1973.
[11] C. Wu and N. F. Rul'kov, "Studying chaos near one-dimensional maps: A tutorial," *IEEE Trans. Circuits Syst. (Special Issue on Chaos in Nonlinear Circuits)*, this issue.
[12] J. M. T. Thompson and H. B. Stewart, *Nonlinear Dynamics and Chaos*. New York: Wiley, 1986.
[13] C. Grebogi, E. Ott, and J. Yorke, "Chaotic attractors in crisis," *Phys. Rev. Lett.*, vol. 48, pp. 1507–1510, 1982.
[14] L. M. Pecora and T. L. Carroll, "Synchronization in chaotic systems," *Phys. Rev. Lett.*, vol. 64, no. 8, pp. 821–824, 1990.
[15] T. L. Carroll and L. M. Pecora, "Synchronizing chaotic circuits," *IEEE Trans. Circuits Syst.*, vol. 38, no. 4, pp. 453–456, Apr. 1991.
[16] M. J. Ogorzalek, "Taming chaos: Part I—Synchronisation," *IEEE Trans. Circuits Syst.*, this issue.
[17] H. Dedieu, M. P. Kennedy, and M. Hasler, "Chaos shift keying: Modulation and demodulation of a chaotic carrier using self-synchronizing Chua's circuits," *IEEE Trans. Circuits Syst.*, this issue.
[18] A. V. Oppenheim, G. W. Wornell, S. H. Isabelle, and K. M. Cuomo, "Signal processing in the context of chaotic signals," in *Proc. IEEE ICASSP*(San Francisco, CA), 1992, pp. IV-117–IV-120, 1992, vol. IV.
[19] A. V. Oppenheim, A. S. Willsky, and I. T. Young, *Signals and Systems*. Englewood Cliffs, NJ: Prentice-Hall, 1983.
[20] A. V. Oppenheim and R. W. Schafer, *Digital Signal Processing*. Englewood Cliffs, NJ: Prentice-Hall, 1975.
[21] W. H. Press, B. P. Flannery, S. A. Teukolsky, and W. T. Vetterling, *Numerical Recipes in C*. Cambridge, UK: Cambridge University Press, 1988.
[22] E. O. Brigham, *The Fast Fourier Transform*. Englewood Cliffs, NJ: Prentice-Hall, 1974.
[23] L. O. Chua, *Introduction to Nonlinear Network Theory*. New York: McGraw-Hill, 1969.
[24] ——, "The rotator—A new network component," *Proc. IEEE*, vol. 55, no. 9, pp. 1566–1577, Sept. 1967.
[25] ——, "Synthesis of new nonlinear network elements," *Proc. IEEE*, vol. 56, no. 8, pp. 1325–1340, Aug. 1968.
[26] L. O. Chua, J. B. Yu, and Y. Y. Yu, "Negative resistance devices," *Int. J. Circuit Theory Appl.*, vol. 11, pp. 161–186, Aug. 1983.
[27] ——, "Bipolar-JFET-MOSFET negative resistance devices," *IEEE Trans Circuits Syst.*, vol. 32, pp. 46–61, Jan. 1985.
[28] L. O. Chua and F. Ayrom, "Designing nonlinear single op-amp circuits: A cookbook approach," *Int. J. Circuit Theory Appl.*, vol. 13, pp. 235–268, July 1985.
[29] M. P. Kennedy, "Robust op amp realization of Chua's circuit," *Frequenz*, vol. 46, no. 3–4, Mar.-Apr. 1992.
[30] ——, "Synthesis of continuous piecewise-linear resistors for Chua's circuit family using operational amplifiers, diodes, and linear resistors," *Int. J. Circuit Theory Appl.*, vol. 21, no. 5, 1993.
[31] J. M. Cruz and L. O. Chua, "A CMOS IC nonlinear resistor for Chua's circuit," *IEEE Trans. Circuits Syst.*, vol. 39, no. 12, pp. 985–995, Dec. 1992.
[32] ——, "An IC diode for Chua's circuit," *Int. J. Circuit Theory Appl.*, vol. 21, no. 2, Mar./Apr. 1993.
[33] M. Delgado-Restituto and A. Rodriguez-Vasquez, "A CMOS monolithic Chua's circuit," *J. Circuits Syst. Comput.*, vol. 3, no. 2, June 1993.
[34] Analog Devices, Inc., *Linear Products Databook 1990/91*, 1990.
[35] T. S. Parker and L. O. Chua, "INSITE—A software toolkit for the analysis of nonlinear dynamical systems," *Proc. IEEE*, vol. 75, no. 8, pp. 1081–1089, 1987.
[36] ——, *Practical Numerical Algorithms for Chaotic Systems*. New York: Springer-Verlag, 1989.
[37] B. Johnson, T. Quarles, A. R. Newton, D. O. Pederson, and A. Sangiovanni-Vincentelli, "SPICE3 version 3e user's manual," ERL Memo., Electron. Res. Lab., Univ. of California at Berkeley, 1991.
[38] Analog Devices, Inc., "SPICE model library, Release C 1/91, 1991.
[39] T. S. Parker and L. O. Chua, "The dual double scroll equation," *IEEE Trans. Circuits Syst.*, vol. CAS-34, no. 9, pp. 1059–1073, 1987.
[40] S. Wu, "Chua's circuit family," *Proc. IEEE*, vol. 75, no. 8, pp. 1022–1032, 1987.
[41] P. Bartissol and L. O. Chua, "The double hook," *IEEE Trans. Circuits Syst.*, vol. 35, no. 12, pp. 1512–1522, 1988.
[42] C. P. Silva and L. O. Chua, "The overdamped double scroll family," *Int. J. Circuit Theory Appl.*, vol. 16, no. 7, pp. 223–302, 1988.
[43] L. O. Chua and G. N. Lin, "Canonical realization of Chua's circuit family," *IEEE Trans. Circuits Syst.*, vol. 37, no. 7, pp. 885–902, 1990.

Michael Peter Kennedy, for a photo and biography, please turn to page 656 of this issue of this TRANSACTIONS.